Design and synthesis of amino acid derivatives of substituted benzimidazoles and pyrazoles as selective Sirt1 inhibitors

Nikil Purushotham[a,$], Mrityunjay Singh[b,c,$], Bugga Paramesha[b,$], Vasantha Kumar[a], Sharad Wakode[c], Sanjay K Banerjee[b,*#], Boja Poojary [a,*], Shailendra Asthana[b,*]

[a]Department of Studies in Chemistry, Mangalore University, Mangalagangotri, Karnataka-574 199, India.

[b]Translational Health Science and Technology Institute (THSTI), Faridabad, Haryana-121001, India.

[c]Delhi Institute of Pharmaceutical Sciences and Research, DPSR University, M.B Road, Pushp Vihar, Sector 3, New Delhi -110017.

Present address: Department of Biotechnology, National Institute of Pharmaceutical Education and Research (NIPER), Guwahati-781101, India

$ These authors contributed equally.

*To whom the correspondence should be addressed:

Dr. Sanjay K Banerjee
Translational Health Science and Technology Institute (THSTI),
NCR Biotech Science Cluster, 3rd Milestone
Faridabad – Gurgaon Expressway, Haryana-121001, India
E-Mail: skbanerjee@thsti.res.in

Dr. Boja Poojary
Department of Chemistry
Mangalore University
Mangalagangotri-574 199.
Karnataka, India
E-Mail: bojapoojary@gmail.com

Dr. Shailendra Asthana
Translational Health Science and Technology Institute (THSTI),
NCR Biotech Science Cluster, 3rd Milestone
Faridabad – Gurgaon Expressway, Haryana-121001, India
E-Mail: sasthana@thsti.res.in

ABSTRACT

Owing to its presence in several biological processes Sirt1 served as a potential therapeutic target for many diseases. Here we report the synthesis of two distinct series of novel Sirt1 selective inhibitors, benzimidazole monopeptides and 5-pyrazolyl methylidene rhodanine carboxylic acid derived amino acids, constructed using structure-guided computational approaches. Furthermore, compounds were evaluated, against human Sirt1-3 for *in-vitro* inhibitory activity compared to Ex527 (reported Sirt1-selective inhibitor), in liver and breast cancer cell lines for cytotoxicity. The tryptophan conjugates 13h (IC_{50} = 0.66 µM) and 7d (IC_{50} = 0.77 µM) demonstrated maximum efficacy to inhibit Sirt1. Molecular dynamics simulations unveil the interaction map and electrostatic complementarity at substrate binding site, could be a cause of selective Sirt1 inhibition. Furthermore, the Sirt1 inhibition was monitored via increased p53 acetylation status checked in HepG2 cells. These findings will pave the pathway for developing novel selective Sirt1-inhibitors in cancer therapeutics.

Key words: Selective inhibitor, Sirtuins, Structure activity relationship, Molecular dynamics simulations, Electrostatic surface potential, hot-spot, drug discovery.

INTRODUCTION

Epigenetic regulation is a dynamic and reversible process which can contribute to a broad range of human diseases that includes metabolic, neurological diseases, inflammation and cancer.[1] In the recent past decade, human homologues of yeast Silent information regulators 2 (Sir2), a class-III lysine deacetylases, also called sirtuins that use NAD^+ as the co-factor to catalyse the deacetylation of several key cellular histone and non-histone proteins[2], have emerged as targets for several diseases along with cancer chemotherapy[3, 4]. Among a total of seven Sir2 homologs (Sirt1-7) found in mammals, Sirt1, Sirt6 and Sirt7 are predominantly found in the nucleus, Sirt2 in the cytoplasm and Sirt3, Sirt4 and Sirt5 in mitochondria.[5] All sirtuins have highly conserved NAD-binding, and catalytic core domain with distinct N- and C-terminal extensions[6-8]. The length of dissimilar N- and C-terminal vary according to the type of binding partners, and its subcellular localization.[6-8] Among all sirtuins, Sirt1's inhibition gain more attention in the recent years for its role in cancer[3], rheumatoid arthritis[9, 10], HIV[10, 11] and autophagy[12].

Sirt1 is the most extensively studied, longest isoform of sirtuins family. It has the NAD^+ binding catalytic core, which can be further divided into two sub-domains, the Rossmann fold (large) and Zn-binding (smaller) domains. The well-characterized catalytic grove is located at the interface of both sub-domains, where deacetylation of the substrates occurs and most of the reported inhibitors are bound[13]. It deacetylates several non-histone proteins and transcription factors *viz.* p53[14], forkhead box class O (FoxO)[15], nuclear factor κB (NFκB)[16], peroxisome proliferator-activated receptor-γ (PPARγ)[17], transcriptional co-activator PPARγ coactivator-1α (PGC-1α)[18], Ku70/XRCC6[19] and histones[7] such as H1, H3 and H4, and regulate their function or energy homeostasis.[20] Therefore, Sirt1 activation, as well as inhibition, appears as attractive and potential mechanisms to combat various diseases associated with aging, metabolic disorder, HIV, neurological disorder and cancer.[11, 20, 21]

The role of Sirt1 in cancer begins from the finding that, it deacetylates p53 and E2F1, and finally inhibit the apoptosis *via* modulation of transcriptional activity. Indeed, the role of Sirt1 in cancer is debatable as in some type of cancers it promotes tumorigenesis[22], while in others like colon cancer, it acts as a tumor suppressor.[22] Though, the mechanism is not yet known, more exploration is under way to find the role of Sirt1 inhibitors in cancer progression.[23, 24] Recently, some Sirt1 inhibitors are reported in an adjuvant therapy for the treatment of paclitaxel-resistant

human cervical cancer[25] and cisplatin-resistant endometrial carcinoma[26]and other cancers[27], thus opened up a new avenue to explore the role of Sirt1 inhibitors in resistant cancer cells**.**

Even though sirtuin's biochemistry has been extensively studied, and many co-crystal structures of several human sirtuin isotypes with inhibitors have been reported till date, due to high amino acid conservity and structural similarity of the catalytic core among sirtuin family members, most of the inhibitors are non-specific and of low micromolar potency *viz.* Sirtinol, Salermide, Suramin and Cambinol.[28-30] In recent years, some isotype-selective sirtuin inhibitors are reported (see **Figure 1** for representative structure) but, most of them are Sirt2 selective.[29] The pyridine containing inhibitor **1**[31]**,** tryptophan-containing Javamide-II **(2)**[32], 2,3-disubstituted benzimidazole-5-carboxylates **3**[33], SirReal **(4)**[34], a compound containing substituted 2-aminothiazole-carboxamide linked to a pyrimidine moiety; thienopyrimidinones **(5)**[35], carboxamide containing AEM2 **(6)**[36] and AGK2 **(7)**[37] are reported as highly Sirt2 selective inhibitor. While in case of Sirt1, only two reported inhibitors, carboxamide containing indole (**8)**[38] and pyrazole **(9)**[39]are known to show moderate Sirt1 selectivity. Similarly, ELT-11c (**10**)[40], a thienoprimidine analog with coreboxide functionality, is one of the most potent Sirt3 inhibitors reported to date, but is non-selective. Therefore, there is a need to develop more selective Sirt1 inhibitors. Though some recent reports highlighted the link between Sirt1 inhibitor and cancer regulation, there is no information regarding the requirement of selectivity of Sirt1 inhibition for anticancer activity[41, 42]. So far, validation of Sirt1 inhibition for anticancer activity has been hindered by the lack of potent and isotype-specific inhibitor.

In the recent developments in drug design, strategically conjugating amino acid fragments to bioactive heterocycles have proved enhancement of desirable pharmacological features such as low toxicity, high bioavailability, stability and cell permeability with modest potency due to its biocompatibility.[43] Fascinated by the above-mentioned findings of the inhibitory potential of some 1,2-disubstituted benzimidazole-5-carboxylates and pyrazoles, respectively, along with the significance of incorporating amino acid fragments in bioactive heterocyclic motifs, we explored the potential of some benzimidazole monopeptides and amino acid derived rhodanine carboxylic acid conjugates with pyrazoles as Sirt1 inhibitors. Here, we are reporting the design and synthesis of 1,2-disubstituted benzimidazole monopeptides *via* one-pot reductive cyclization method and rhodanine acid conjugated pyrazoles via Knoevenagel condensation reactions, and investigation of their Sirt1 inhibitory potential in cell-free and cell-based assays and the plausible mechanism of

inhibition through molecular dynamics simulations. The selective Sirt1 inhibition was also correlated with anticancer activity in two different cell lines.

RESULTS AND DISCUSSION

Chemistry:

The synthetic strategy of novel benzimidazole monopeptides is depicted in **Scheme 1**. Initially, ethyl 4-chloro-3-nitrobenzoate **(2)** was prepared by esterification of 4-chloro-3-nitrobenzoic acid **(1)** in refluxing ethanol with a catalytic amount of sulphuric acid. The resulting ester was subjected to nucleophilic aromatic substitution with cyclohexylamine in THF using triethylamine as the base at room temperature to obtain ethyl 4-cyclohexylamino-3-nitrobenzoate **(3)**. Successively, the benzimidazole core was accomplished by sodium dithionite assisted reductive cyclization of ethyl 4-cyclohexylamino-3-nitrobenzoate **(3)** with substituted benzaldehydes in DMSO at 90 °C. The benzimidazole esters **(4a-c)** were then hydrolyzed to the corresponding carboxylic acids **(5a-c)** in refluxing aqueous sodium hydroxide solution. These benzimidazole carboxylic acids, when coupled with various amino acid methyl ester hydrochlorides, in presence of *N*-methyl morpholine using TBTU as the coupling agent in DMF media, furnished ester protected benzimidazole monopeptides **(6a-l)**. These monopeptide esters were hydrolyzed to obtain the target benzimidazole monopeptides **(7a-l)** using lithium hydroxide monohydrate in THF-water mixture at 0 °C.

The synthetic strategy for the rhodanine carboxylic acid conjugated pyrazoles is depicted in **Scheme 2**. In order to synthesize the final compounds, the two key scaffolds (i) pyrazole aldehyde and (ii) rhodanine acids were initially prepared separately. For the preparation of 3-substituted-1*H*-pyrazole-4-carboxaldehydes, appropriately substituted acetophenones **(8a-c)** were heated with semicarbazide hydrochloride in the presence of sodium acetate in acetic acid to obtain the corresponding semicarbazones **(9a-c)**. These on cyclization with phosphorous oxychloride *via* Vilsmeier Haack reaction furnished 3-substituted-1*H*-pyrazole-4-carboxaldehydes **(10a-c)**. For the preparation of rhodanine acetic acids **(12a-d)**, suitable amino acids **(11a-d)** were initially dissolved

in an aqueous solution of potassium hydroxide and treated with carbon disulfide to obtain the corresponding potassium salt of dithiocarbamates. These on treatment with potassium chloroacetate, followed by heating with 2N HCl solution yielded the 2-(4-oxo-2-thioxothiazolidin-3-yl)-amino acids **(12a-d)**. Finally, the two key scaffolds were clubbed together by means of Knoevenagel condensation using beta-alanine as the catalyst to accomplish the target compounds **(13a-l)** in good yield.

Binding evaluation of all the compounds through Docking and MM-GBSA calculations:

Accurate prediction of *binding-site* and *binding-mode* in protein is challenging, however, identification of accurate binding mode inside the binding site is the prerequisite for designing more selective molecules. In order to investigate the structural requirements involved in the amino acid derivatives of benzimidazole and pyrazole class of compounds, we synthesized a total 24 compounds derivatives, 12 from each group, *via* structure-guided substitution of diverse functionalities to rationalize the Sirt1-inhibitory activity of these compounds in terms of structural modifications. The compounds were first evaluated by molecular docking, followed by thermodynamic calculations through MM-GBSA. The molecules that appeared promising in their docking and MM-GBSA scores were selected for further biological evaluation. Thereafter, molecular dynamics simulations (MD) was performed to prepare the SAR based on stable architecture of binding site and orientations of binding residues to understand the molecular mechanism for selectivity and biological outcomes.

The Ex527 and its analog (Ex527*) belong to the same chemical class and have nearly same binding affinity and IC_{50} values (IC_{50_EX527} = 92 µM, IC_{50_4I5} = 124 µM), therefore the PDB "4I5I" was selected as a reference for model building, docking and simulation studies. Initially, focused docking and MM-GBSA calculations were performed for Ex527 and Ex527*, by using the centre of mass of Ex527* as a grid centre to check the system reproducibility and benchmark studies (**Table S1**). It was reported that, inhibitor binding site in sirtuins was flexible and dynamic in nature[34]; therefore, we considered the flexibility of the sirtuin's catalytic and inhibitor binding site and performed MD simulations of Sirt1-Ex527* complex and the best docked pose of Sirt1-Ex527 complex, to get the exact binding modes of Ex527 and Ex527*. The overlaid structures (the average structure extracted from last 80 ns of total 200 ns MD simulation of each) had shown that both Ex527 and Ex527* were bound at the same place (complex RMSD 0.98 Å), nested deep

within the active site, and primarily interacted through pi-pi, hydrophobic and hydrogen bond interactions (**Figure 2A and S1**). The MM-GBSA ($-\Delta G_{bind}$) and docking scores of Ex527 and Ex527* were -60.00 kcal/mol and -6.0 respectively (Table1). Therefore, we took the docking score (-6.0) and $-\Delta G_{bind}$ (-60.0 kcal/mol) as cut-off values for the selection of compounds for further analysis (**Figure 2B**). Furthermore, after setting the benchmark and cut-off values, the focused docking and MM-GBSA calculations at the above-mentioned grid centre were performed to re-score our library of synthesized molecules. A total of twenty-four amino acid-heterocycle conjugates were designed and synthesized using a combination of various amino acids and two types of heterocyclic scaffolds, namely, benzimidazole and pyrazole. Out of the two series, Series1 consisted of twelve substituted benzimidazole monopeptides derived from four amino acids *viz.* Alanine, Valine, Leucine and Tryptophan (**Scheme1, Table 1**), whereas, Series2 consisted of twelve substituted pyrazolyl methylidenes of rhodanine carboxylic acids derived from four amino acids *viz.* Glycine, Alanine, Phenylalanine and Tryptophan (**Scheme2, Table 2**). A ligand library of total 540 lowest energy conformations was generated from these 24 designed compounds and used for focused docking. Furthermore, MM-GBSA calculations and rescoring were done by Induced Fit docking module, with consideration of protein flexibility up to 5.0 Å to get the most likely orientation of each compound (**Table 1 and 2)**. The compounds qualified to cross the cut-offs are 7a, 7b, 7c, 7d, 7g and 7h (from Series1) and 13d, 13h and 13l (from Series2) were selected for further cell-based biological evaluation.

Evaluation of Inhibitory Activity:

Enzyme-based study. All compounds selected from **Table 1 and 2**, initially screened for their inhibitory activity against Human recombinant Sirt1-3 with an *in-vitro* enzyme-based assay by using Enzo life sciences (Cat No.BML-AK555 for Sirt1, Cat No. BML-AK556 for Sirt2 and Cat No. BML-AK557 for Sirt3). We followed manufacturers' protocol to perform the assay at 10 µM concentration using Ex527 as a positive control and DMSO as a negative control. The fluorescently labelled p53-K382 was used as a substrate to measure Human recombinant Sirt1 activity and labelled p53-K320 to measure Human recombinant Sirt2 and Sirt3 activity. At 10 µM concentration, Ex527 (positive control) showed inhibition of 98% (Sirt1), 70% (Sirt2) and 77% (Sirt3) (**Table S1**). However, most compounds showed maximum inhibition activity against Sirt1 and very moderate inhibition activity against Sirt2 and Sirt3. Four compounds 7d, 13d, 13h and

13l had shown almost 90% inhibition against Sirt1 which was comparatively close to the positive control (**Table 1 and 2**).

Cell-based study. Further, to validate the results of enzyme-based assay, we performed cell-based Sirt1-3 enzyme inhibition activity. For this, we treated the HepG2 cells with test compounds at a concentration of 10 µM for about 12 h and followed by evaluation of Sirt1-3 enzymatic activity. In cell-based assay, we found that four compounds 7d, 13d, 13h and 13l showed Sirt1 inhibition (≥30%) effect similar to positive control Ex527 (33% Sirt1 inhibition), while compounds 7a, 7b, 7c, 7g and 7h showed moderate or less inhibitory activity against Sirt1-3 (**Table 3**). Compounds 7d, 13d, 13h, and 13l showed Sirt1 activity inhibition of 38%, 36%, 48%, and 30%, respectively. Among all the compounds, 13h showed exceptionally high activity against Sirt1, and the inhibition activity trend was 13h>7d>13d>13l. In case of inhibition of Sirt2 and Sirt3 activity together (because of same substrate for both sirtuin's), we observed that compounds 13d, 13h, and 13l showed mild inhibition of 6%, 10% and 9%, respectively, which was very less than activity inhibition showed by Ex527 (Sirt2 and Sirt3 inhibition 15%). Similar to Ex527, compound 7d also exhibited Sirt2 and Sirt3 inhibition of 19%. Our study showed that compounds 13d, 13h and 13l were more selective towards Sirt1, while 7d is more towards Sirt2 and Sirt3 in comparison to Ex527.

Dose-response study. Based on the cell-based Sirt1 inhibition activity study, active compounds 7d, 13d, 13h and 13l were selected for dose-response study by using human recombinant Sirt1; and their IC_{50} values were calculated by using different concentrations of test compounds. Ex527 was used as the standard to compare with the test compounds. Ex527 was used as the standard to compare with the test compounds. Ex527 showed IC_{50} 0.60+0.02 µM while our test compounds 7d, 13d, 13h and 13l showed IC_{50} values 0.77+0.04 µM, 0.71+0.03 µM, 0.66+0.02 µM and 0.73+0.06 µM, respectively (**Table 3)**.

Viability assay on cancer cell lines. Further to check the anticancer property of our test compounds, two human cancer cell lines, HepG2 (Human liver cancer cell line) and MCF7 (Human breast cancer cell line) were used. To find out the cytotoxicity towards cancer cell lines, MTT assay was performed on both cancer cell lines. We treated the cancer cell lines with different concentrations of our test compounds and Ex527 (1 µM to 400 µM) for about 24 h. Then we

performed the cell viability assay and % viability was calculated. In HepG2 cells, Ex527 and compound 7d both exhibited a continuous decrease in cell viability with increasing inhibitor concentration while, compound 7d showed moderate decrease in cell viability at higher concentration and, compounds 13h and 13l showed comparably very less decrease in cell viability among all compound tested (**Figure 3A**). In MCF7 cells, 7d similar to the HepG2 cell line showed continuous/comparatively higher decrease in cell viability with increasing inhibitor concentration. However, Ex527 and other test compounds 13d, 13h, and 13l, showed no significant changes in cell viability (**Figure 3B**).

It was reported earlier that inhibition of Sirt1 and Sirt2 together is necessary for cell death or apoptosis, while selective inhibition of Sirt1 only induced cell cycle arrest at G1-phase but not cell death[44, 45]. This means Sirt1 selective inhibition along with Sirt2 inhibition is essential for cytotoxic activity[46], our data confirmed the same findings. Our cell-based assay showed that both Ex527 and 7d having Sirt2 and Sirt3 inhibition 15% and 18%, respectively at 10 µM concentration. As the compound 7d has higher Sirt2 and Sirt3 inhibition than control Ex527, it showed higher cell death in both types of cancer cell lines, HepG2, and MCF7. Since, compounds 13d, 13h and 13l were comparatively more selective towards Sirt1 inhibition, showed very less cell death in cell viability (MTT) assays.

Acetylation status of p53. p53 plays an important role in cancer cell's survival and death. The acetylated form of p53 binds with the DNA and induces the expression of several apoptotic genes and thus acts as a tumor suppressant.[47] It was reported that Sirt1 primarily deacetylate C-terminal lysine residue (K382) of p53 and enables p53 to bind with DNA, thereby increasing p53 transcriptional activity[48]. So here we wanted to check the acetyl-p53 levels in HepG2 cells in presence of Sirt1 inhibitors that we have designed and positive positive control. We treated the HepG2 cells with 25 µM of test compounds for about 48 h. Cell lysates were used for immunoblotting. We found that 7d increased the Ac-p53 levels in HepG2 cells comparable to the positive control, Ex527 (**Figure 3C).**

These assays outcomes helps to decipher us that 13h standout as a Sirt1 selective molecule in comparison with Ex527, and compound 7d can be explore futher as anticancer molecule as it is significantly inhibiting the Sirt1 and moderatly inhibiting Sirt2 as well, which is a prerequsite property of a anticancer molecule. (Figure 3).

Dynamics of protein-ligand systems:

RMSD pattern reflects the dynamics stability of the systems. To rule out the limitations of molecular docking and to understand the molecular recognition process, the role of solvation, the 200 ns long MD simulations were carried out for each system. Another fact to carry out the MD simulation, as the binding site of Sirt1 is highly flexible in nature and it is solvent exposed, therefore, static docking has limitation to interpret binding affinity and stability. The energy minimized apo and complexes of selected compounds (7d, 13d, 13h and 13l) and the control (Ex527) with Sirt1 were used for subsequent MD simulations. The RMSD of each complex was compared with that of the apo protein. All the complexes showed stable $RMSD_{avg}$ ~2.5 Å, which was considerably lower than the apo system $RMSD_{avg}$ 3.5 Å, and control system, Sirt1-Ex527 $RMSD_{avg}$ is 3.0 Å, indicating that binding of selected compounds has shown a promising effect in the stability of systems. (**Figure 4A**). The average RMSD of complex systems Sirt1-7d, Sirt1-13d, Sirt1-13h and Sirt1-13l were 2.5 Å, 2.8 Å, 2.1 Å and 2.8 Å, respectively. Since complex Sirt1-13h is the most stable complex among all, it has shown the lowest, smooth and unimodal RMSD distribution. Although, complex Sirt1-13d and Sirt1-13l both had nearly same average RMSD, which was highest among complex systems (Sirt1-7d, Sirt1-13d, Sirt1-13h, Sirt1-13l); But Ligand RMSD distribution plot for Sirt1-13l was bimodal while for Sirt1-13d it was unimodal. The bimodal RMSD distribution has shown fluctuation in RMSD and since complex Sirt1-13l unstability increased after 100 ns from 2.5 Å to 3.0 Å, it was noticed that Sirt1-13d is more stable. In cell-based assay the biological inhibitory activity pattern 13h>7d> 13d> 13l, corroborates well with computational outcomes (**Figure 4A**, MD stability, 13h>Ex527~7d> 13d> 13l).

Binding of compounds perturbed the dynamic fluctuations. To identify the regions in protein Sirt1 which had gained stability in the complexes, we have performed root mean square fluctuation (RMSF) analysis. The average backbone RMSF value and differences in RMSF (ΔRMSF) for system Sirt1-Ex527 and Sirt1-7d relative to the apo-system are quantified (**Figure 4B)**. The regions 270-310 that belonged to pocket-C, indicated a significant decrease in RMSF in both the complex systems, Sirt1-Ex527 and Sirt1-7d, compared to the apo-system. Similarly, another region 410 to 460 which belongs to the substrate binding site also reflected substantially decrease in RMSF, in both the complexes. Moreover, Sirt1-7d has shown significant drop in the regions

260-310 and 410 to 460 than Sirt1-Ex527* (Control); henceforth these regions were considered for further analysis. Interestingly these regions were also used earlier for the designing of inhibitors[40, 49]; So, pocket-C and substrate binding sites were selected as two hot-spots for structure-based ligand optimization and protein-ligand interaction studies. The region belonging to pocket-C was called *hot-spot1* while the region belonging to the substrate binding region was denoted as *hot-spot2* in this study (**Figure 4B**).

Per-residue energy decomposition revealed key residues of the binding sites. The per-residue energy decomposition claimed that in Ex527* (control), a total 9 residues (S265, I270, F273, I279, F297, I316, N346, I347 and I411) reflected major contribution in binding free energies ($\Delta G_{pbsa} \leq$ -0.5 kcal/mol), and among them I347 and N346 contributed highest (Figure **4C**). However, in the case of compounds 7d and 13h, around 12 residues showed major contribution to binding free energy ($\Delta G_{pbsa} \leq$ -0.5 kcal/mol) (**Figure 4C**). In 7d, residues, A262, F273, D292, F297, I347, E351, H363, V412, F414, L418, V445 and R446 reflected major contribution in binding free energy and among them F273, H363 from pocket -B & -C, and L418 and R446 from hot-spot2 contributed highest (**Figure 4C and 4D**). Similarly, in case of 13h, residues D272, F297, Q345, I347, H363, I411, V412, F413, F414, L418, V445 and R446 showed major contribution and among them, F297, I347, H363 form pocket-B and pocket-C and V412, F413 and F414 from substrate binding site, contributed highest (**Figure 4C and 4D**). We observed that in Ex527* all 9 residues that played a key role in interaction belong to pocket -B & -C only and no interaction was observed with residues at substrate binding site. While in case of 7d and 13h both, residues from all three sites, pocket – B & -C and substrate binding site played major role in interaction (**Figure 4C**). The residue wise interaction analysis also claims that 7d has shown the maximum interaction at NAD^+ site and pocket-C, while in the case of 13h, it was gained at the substrate site.

Establishment of Structure-Activity Relationship (SAR):

Structural study of complex Sirt1-Ex527. As reported by Mellini P et al.[49] and others, the catalytic groove was well differentiated into three sub-pockets, pocket A (substrate-binding site), B (NAD^+-binding site/I-shaped) and C (NAM binding-pocket).[40, 49](**Figure 2A**). In terms of key residues, we identified the area around the residue F414 is denoted as pocket A and interacts with the acetylated lysine of the substrate; region below the residue R274 is denoted as pocket B and

co-factor NAD/ADPR bind in this pocket; region beneath the residue F273 is denoted as pocket C, also called NAM-binding pocket, and is very critical for deacetylase activity[13, 34] (**Figure S1A**). Inhibitors Ex527 and Ex527* (Ex527-analogue) both bind into the pocket-C and hinder the transformation of NAD to L-shape which is required to perform deacetylase function[13]. The pocket-C is made up of two types of residues hydrophobic and polar. Residues F273, Y280, and I347 that covers it from the front- and side- face are forms pi-pi and hydrophobic interactions. Residues, Q345, N346, and D348 form the base of pocket-C and established polar electrostatic interactions (**Figure S1B**). Both types of interactions appeared necessary for the inhibitory activity of Ex527 and Ex527*.

Structure-activity relationship of both series of compounds. We found that among all synthesized compounds only 7d, 13d, 13h and 13l, which had 1*H*-indole substitution at -R_2 position, showed good results in cell-based assay in HepG2 cells (**Table 3)**. As shown in 3D interaction map in **Figure 4D**, the indole moiety of compound 7d, 13d, 13h and 13l, localized in C-site and established pi-pi interaction with residue F273, hydrophobic contacts with residues I270, P271 and I347 and polar interactions with residues S265, Y280, Q345, and N346. From the comparison of 2D interaction plot, we found that these compounds have shown interaction maps similar to control Ex527* and Ex527 at pocket –C (**Figure S1B and S2**). From the interaction map, it was found that the binding of polar and aromatic groups like indole moiety at pocket-C seems to be necessary for the inhibitory activity of the compounds. The MD simulations revealed that some residues at substrate binding site/*hot-spot2* also crucial as they contribute significantly in the stability of compounds and lower down RMSF fluctuation in complex Sirt1-7d compared to control Sirt1-Ex527* and Sirt1-apo. (**Figure 4B**). Further, we also measured the interaction fraction analysis for all complexes and control (**Figure S3**). The results of interaction fraction analysis validate the outcome of RMSF, and clearly reflected that 7d, 13d, 13h and 13l have additional interaction zone, the substrate site (pocket-A, *hot-spot2*) compared to Ex527. We observed that at substrate site most of the interactions are electrostatic (HBs, water bridges and ionics) and dominate the overall interaction contribution in 13d and 13l (**Figure S3**). As shown in **Figure 4D** residues, the aromatic residue H363 and substrate binding residues (412-419 and 442-449) jointly formed *hot*-spot2. At *hot*-spot2, aromatic residues H363 and F414 formed pi-pi or pi-cation interaction with benzimidazole moiety of 7d and, pyrazole and rhodanine moiety of 13d,

13h and 13l; residues L418, V445 formed hydrophobic contact with R_1 substituted phenyl moiety, and, the small substitution of 4–OMe/4-NO_2/2-Cl-6-F at R_1-position, was found to be good for the stability of compounds formed polar, water bridge or direct h-bond contact with basic residue K444 and R446. (**Figure 4D and S3**). Further analysis of the 2d interaction plot (**Figure S2**) also revealed that compounds 13d, 13h and 13l exceptionally form pi-cation interaction with residue F413, which was absent in case of compound 7d, that could be a reason for more sirt1 selectivity of compound 13d, 13h and 13l. Moreover, **Figure 4D** reflected that in all three 13d, 13h and 13l, residue R274 and Y280 formed either direct h-bond or water bridge contact with carboxylic acid moiety at pocket-B, which was missing in case of 7d due to structural orientation, could be a reason for higher affinity and Sirt1 selectivity of 13d, 13h and 13l. These observations are consistent with the Sirt1 selectivity pattern of compounds of pyrazole group *viz*. 13h and benzimidazole group 7d in biological assay.

The structural analysis of docked Sirt1 complexes of 7d, 13d, 13h and 13l reflected that in both benzimidazole and pyrazole class of compounds, the -R_1 substitution localized toward the solvent face of substrate pocket and the substitution -R_2 is protruded towards the pocket-C (**Figure 4D**). Similarly, when we superimposed the best docked poses of all the compounds of benzimidazole monopeptide class (**Table 1**), which had 4-OMe at -R_1 substitution, with complex 7d, we found that the polar aromatic indole moiety which appeared to be crucial for the interaction, was missing in other compounds (**Figure 5A**), could be a possible reason for the loss of their inhibitory activity. Similarly, as shown in **Table 1** three compounds 7d, 7h and 7l from benzimidazole class had indole group at -R_2 position that was required for the inhibition of Sirt1 biological activity as predicted above, but among them, only 7d was found to be active in cell-based assay system (**Table 3**). We observed that compounds 7d, 7h and 7l only differ in substitution at R_1 position (**Figure 5B, Table 1**), and compound 7d which had 4-OMe at R_1 position showed good inhibition of Sirt1 catalytic activity. In case of compound 7l, R_1 substitution was "2-Cl", which was at ortho position, and -Cl substitution at ortho position formed steric clash with residue L418 and decreased the MD stability of compound (**Figure 5B and 5C**), Similarly, in case of compounds 7h the R_1 substitution was 4-F (**Figure 5B**). During MD simulation it was found that compound 7h was comparatively less stable than 7d, (**Figure 5C**).

Interestingly, as shown in **Figure 4D** the upper hydrophobic groove which is flexible and made by residues V412 to P419 makes a flexible groove in which phenyl moiety of 7d was trapped

completely and providing the gain in binding affinity. *This groove is a narrow hydrophobic pocket, which could be an area of future exploitation to find additional classes of selective Sirt1 inhibitors.* Apart from 7d series, till now none of the inhibitors are able to utilize this groove as it is mostly unavailable due to its flexibility and its vicinity with the substrate binding site. Also, the compound 13h gain additional interaction in the form of stable HBs/water bridge or polar contact by its di-fluoro group with basic residue K444 and R446 (**Figure S3C**) that is not reported earlier for any compounds at substrate site that is the interaction with di-fluoro group of 13h with R446. This appears, as unique property in case of selectivity as K444 and R446 are present in Sirt1 only (in place of K and R it is Q/E in Sirt2/3, respectively). Similar interaction also formed in 7d but was comparatively weak and transient (**Figure S3C**).

Possible mechanism of Inhibition:

To get structural insights into the possible inhibition mechanism of identified compounds, we compared our compound 7d and 13h with the co-crystal structures of other reported best potent sirtuin inhibitor which either in orientation or in size occupying the binding sites, similar to our compounds *viz.* Ex527* (control, 8), SirReal2 (4) and ELT-11c (10) of different sirtuin analogs, Sirt1, Sirt2 and Sirt3, respectively (**Figure S4**). The Ex527* binds only in the pocket-C (PDB id. 4I5I), SirReal2 (PDB id. 4RMG) binds in pocket-C and extended selectivity pocket-C, while ELT-11c (PDB id. 4JSR) binds at NAD+ site, pocket-C and substrate-binding site, (**Figure S4A and S4B**). As shown in Figure **S4A and S4B**, the chemical moieties of 7d and 13h such as 4-methoxyphenyl/3,5-difluorophenyl, benzimidazole/pyrazol, thiazole and indole interact with different key zones of Sirt1 starting from substrate site, NAD^+ site, and pocket-C, similar to best reported potent Sirt3 inhibitor ELT-11c, but did not interact with extended pocket-C, unlike SirReal2 (potent, selective Sirt2 inhibitor) which is the key known zone for selective Sirt-2 inhibition. Therefore, we compare the reported compounds for the possible mechanism of inhibition of our compounds as they follow the same pose and mode of interactions. Interestingly, the zone pocket-C, the binding site of Ex527 was common in both ELT-11c and SirReal2 and others reported most of the sirtuin inhibitor of different isoform, indicated towards the necessity of pocket-C for potent sirtuin inhibition but less isoform selectivity. The Ex527 binding site thus enables potent sirtuin inhibition, but for further improvement of Ex527 modifications that possibly

reach more distant for specificity among isoforms will be required. In this regard, we observed that our compounds 13d, 13h, and 13l have more isoform specificity than Ex527.

The overlay of Sirt1 and Sirt3 indicates that the rossmann fold is highly superimposable, and we have observed a fold closure of catalytic binding cavity upon binding to substrates (**Figure S4C and S4E**) while opposite trend was observed on binding with inhibitor (**Figure S4D and S4F)**. The largest divergence among sirtuins structures occurs at the flexible loop I270 to D292 (Sirt1) or I154 to Y175 (Sirt3), which closes down on the nicotinamide C-pocket. The atomic level observation explored the different interactions and establishment of HBs with different residues of substrate site, NAD+ site and residues of pocket-C. From MD simulations we find that at substrate site apart from direct HBs few water-mediated interactions were also observed. The consistent HBs making residues are R274, Q345, H363, E416 and R446. The recognition motif for the nicotinamide of NAD^+ is mimicked very well by 7d and 13h and explains the observed SAR in **Table 3**. As a result, a substantial reduction of Sirt1 inhibitory activity is observed for compounds 7d and 13h.

It's well-known that, electrostatic interactions play a critical role in ligand binding, as protein has a specific electrostatic environment that ligand needs for binding. We compared the Sirt1, Sirt2 and Sirt3 binding sites in terms of electrostatic surface potential (ESP), as the ESP is an important key factor at the region of substrate binding site and played key role in the Sirt1 selectivity and binding of 7d (**Figure 6**). The electrostatic surface potential was calculated via APBS method in scrodinger maestro-2017 for pH 7.5, with a color ramp of ± 0.5, from red to blue. As shown in Figure 6C and 6D, the ESP of 7d is in full complementarity to ESP of binding cavity of Sirt1 and it favor the binding of 7d with Sirt1. Furthermore, we observed that in Sirt1 at substrate binding site residues 442-449 have positive ESP while in case of both Sirt2 and Sirt3 the substrate binding site residues, 263-270 (Sirt2) and 321-328 (Sirt3) have negative ESP and appeared red. Since ligand 7d, 13d, 13h and 13l all have negative electrostatic potential near substrate binding site, the ESP of protein-ligand complex system in Sirt1 reflected complete ESP complementarity that is favorable for binding in protein Sirt1 (**Figure 6E)**, while in case of Sirt2 (**Figure 6F**) and Sirt3 (**Figure 6G**) at substrate binding site, protein and ligand both have negative ESP i.e. Red-red combination that is not favorable for binding, and repel to each other and possibly a cause of decrease affinity of 7d and 13h in Sirt2 and Sirt3. In Sirt1 two basic residue, K444 and R446 have positive ESP ie. protein surface in blue color at substrate binding site and act as a selectivity hot-

spot for interaction, while in case of Sirt2 and Sirt3 the counterpart residues are glutamine (Q265, Q267) and glutamic acid (E321, E325), respectively that make ESP partially negative, and surface of protein appeared red color (**Figure 6)**. This difference in ESP behaviour at substrate binding site in Sirt1, Sirt2 and Sirt3, reflected that the ligand with negative ESP at substrate binding site will be more Sirt1 selective and so, our compounds 7d, 13d, 13h and 13l. Many Sirtuin inhibitors previously, targeted the substrate binding site and/or the NAD^+ pocket for competitive inhibition[30, 50, 51-53], indicated the importance of the substrate binding site for inhibitor designing. From our results, we conclude that substrate binding site (N-ε-acetyl lysine binding site) with pocket-C appears to be a prominent site for inhibitor designing, and neighbouring variations with electrostatic complementarity at substrate binding site may enable more isoform-specific inhibition. This data possibly help to understand conformational changes to design for substrate mimics and other acyl-peptide competitive inhibitors.

CONCLUSION

In summary, two novel series of compounds were designed by conjugating the amino acid moiety to benzimidazole and pyrazole based scaffolds. Both series of compounds were synthesized and evaluated against Sirt1-3 enzymes for their sirtuin inhibitory activity compared to Ex-527. The molecular docking and MM-GBSA calculations of the compounds followed by *in vitro* enzymatic and cell-based assays revealed that the tryptophan conjugates of both scaffolds were potent and highly selective in inhibiting Sirt1 enzyme over the rest of the homologues with nanomolar potency, comparable to the known inhibitor, Ex-527. The *in silico* and *in vitro* based structure activity relationship studies illustrated the need for the compounds to possess a polar aromatic moiety such as indole that can interact with C-pocket and another aromatic ring to interact with A-pocket in Sirt1 catalytic domain to exhibit the inhibitory action. Small substitutions such as methoxy, nitro or difluoro on phenyl ring that falls on the solvent exposed sites of the catalytic domain can further improve the stability and selectivity of the enzyme-inhibitor complex. We found that the improved Sirt1 selectivity of our compounds may be due to the presence of strong electrostatic interactions with the two basic residues K444 and R446 at lower cleft of substrate binding site that favors the interactions with electronegative atoms like O and F via formation of a multiple hydrogen bonds, water bridge and polar contacts. We observed that, although both ELT-11c and our molecules occupied the substrate binding site along with pocket-C, the gain of

selectivity of our compounds may be due to the presence of its interactions and ESP complementarity at substrate binding site. Immuno-blotting of HepG2 cells treated with compounds 7d, 13d, 13h, 13l and Ex527 further confirmed that the decreased Sirt1 enzyme activity is associated with increased acetylated p53 levels. In addition, the cell-viability assay confirmed that on Sirt1 the compounds 13d, 13h and 13l are less effective to kill cancer cells than the compounds 7d and Ex527 which showed a mild inhibition of Sirt2 along with their considerable Sirt1 inhibition. In a nutshell, 13h standout as a Sirt1 selective molecule in comparison with Ex527, and 7d could be explore further as anticancer molecule as it inhibits both Sirt1 and Sirt2. These findings could be helpful for developing a novel selective Sirt1-inhibitors.

EXPERIMENTAL SECTION

Chemistry:

All precursor chemicals and solvents were procured from Spectrochem Pvt. Ltd. (India) and Sigma-Aldrich (India) via commercial vendors in suitable grades and used without further purification. The reactions were conducted with a guard tube containing calcium chloride attached to the reaction flask. Open capillary method was used to determine the uncorrected melting points. Shimadzu FT-IR 157 Spectrometer was used to record the IR spectra. Bruker Avance II - 400 spectrometer was used to record NMR spectra at 400 MHz for ^{1}H and at 100 MHz for ^{13}C nuclei respectively. Tetramethylsilane (TMS) served as an internal standard. The values of coupling constants (*J*) and the chemical shifts (δ) are expressed in Hertz and parts per million (ppm) respectively. Agilent Technology LC-Mass spectrometer with ESI ionization was used to record the mass spectra. Elemental analysis was conducted in CHNS Elementar Vario EL III. Thin layer chromatography (TLC) was carried out on a silica coated aluminium sheet (silica gel $^{60}F_{254}$) to monitor the reaction progress and purity of the compounds using ethyl acetate and hexane solvent systems as mobile phase and visualized under UV light at 254 nm. Column chromatography was performed with 60-120 mesh silica gel.

Procedure for the synthesis of ethyl 4-(cyclohexylamino)-3-nitrobenzoate (3)

To a clear solution of ethyl 4-chloro-3-nitrobenzoate (**2,** 0.01 mol, 1.0 equiv.) in 15 mL of THF, cyclohexylamine (0.02 mol, 2.0 equiv.) and triethylamine (0.03 mol, 3.0 equiv.) were added and stirred at room temperature for 24 h. Progress of the reaction was monitored by TLC. After completion of the reaction, the reaction mixture was quenched with crushed ice and left undisturbed for two hours. The resulting yellow solid was washed with water, filtered and dried. The crude product was recrystallized from ethyl alcohol to obtain the pure product.

Procedure for the synthesis of benzimidazole esters (4a-c)

Sodium dithionite (0.03 mol, 3.0 equiv.) was added to a clear solution of ethyl 4-(cyclohexylamino)-3-nitrobenzoate **(3)** (0.01 mol; 1.0 equiv.) and substituted benzaldehyde **(**0.01 mol; 1.0 equiv.) in DMSO (15 mL). The reaction mixture was stirred at 90 °C for 3 h. After completion of the reaction (monitored by TLC hexane: ethyl acetate (8: 2, v/v)), the reaction mass was allowed to cool to room temperature and poured onto crushed ice. The solid separated was filtered, washed with water, dried and recrystallized from ethyl alcohol to obtain the pure product.

Ethyl 1-cyclohexyl-2-(4-methoxyphenyl)-1H-benzo[d]imidazole-5-carboxylate (4a): Yield 92%; Mp 118-120°C; Off white to pale yellow solid; FT IR (ATR, υ_{max}, cm^{-1}): 3001 (Ar-H), 2933, 2856 (C-H), 1705 (C=O), 1610 (C=N), 1529 (C=C), 1172 (C-O); ^{1}H NMR (400 MHz, $CDCl_3$, δ ppm): 8.52 (d, 1H, Ar-H, *J* = 1.2 Hz), 7.97-7.99 (dd, 1H, Ar-H, *J* = 1.6 and 8.8 Hz), 7.66 (d, 1H, Ar-H, *J* = 8.8 Hz), 7.59 (d, 2H, Ar-H, *J* = 6.8 Hz), 7.07 (d, 2H, Ar-H, *J* = 6.8 Hz), 4.40-4.45 (q, 2H, $-CH_2$ of ethyl, *J* = 7.2 Hz), 4.33-4.39 (m, 1H, N-CH of cyclohexyl), 3.90 (s, 3H, $O-CH_3$), 2.27-2.36 (m, 2H, cyclohexyl), 1.95-1.99 (m, 4H, cyclohexyl), 1.77-1.79 (m, 1H, cyclohexyl), 1.43 (t, 3H, $-CH_3$ of ethyl, *J* = 7.2 Hz), 1.33-1.38 (m, 3H, cyclohexyl); ^{13}C NMR (100 MHz, $CDCl_3$, δ ppm): 167.2, 160.9, 155.5, 143.4, 137.3, 130.8, 124.3, 123.4, 122.8, 122.2, 114.2, 112.0, 60.8, 57.1, 55.4, 31.4, 25.9, 25.2, 14.4; ESI-MS (*m/z*): 379.2 $[M+H]^+$; Anal. calcd. for $C_{23}H_{26}N_2O_3$: C, 72.99; H, 6.92; N, 7.40. Found: C, 72.97; H, 6.94; N, 7.37.

Ethyl 1-cyclohexyl-2-(4-fluorophenyl)-1H-benzo[d]imidazole-5-carboxylate (4b): Yield 87%; Mp 130-132°C; Off white to pale brown solid; FT IR (ATR, υ_{max}, cm^{-1}): 3050 (Ar-H), 2927, 2850 (C-H), 1705 (C=O), 1602 (C=N), 1527 (C=C), 1300 (C-O), 1224 (C-F); ^{1}H NMR (400 MHz, $CDCl_3$, δ ppm): 8.52 (d, 1H, Ar-H, *J* = 1.2 Hz), 7.99-8.02 (dd, 1H, Ar-H, *J* = 1.6 and 8.8 Hz), 7.67 (d, 1H, Ar-H, *J* = 8.8 Hz), 7.62-7.66 (m, 2H, Ar-H), 7.23-7.27 (m, 2H, Ar-H), 4.4-4.45 (q, 2H, -CH_2 of ethyl group, *J* = 7.2 Hz), 4.29-4.35 (m, 1H, cyclohexyl N-CH), 2.27-2.36 (m, 2H, cyclohexyl), 1.95-2.03 (m, 4H, cyclohexyl), 1.76-1.8 (m, 1H, cyclohexyl), 1.43 (t, 3H, -CH_3 of ethyl group, *J* = 7.2 Hz), 1.35-1.36 (m, 3H, cyclohexyl); ^{13}C NMR (100 MHz, $CDCl_3$, δ ppm): 167.1, 164.9, 162.5, 154.4, 143.3, 137.1, 131.5, 131.4, 126.8, 124.6, 123.7, 122.46, 116.0, 115.9, 112.1, 60.8, 57.3, 31.5, 25.9, 25.2, 14.4; ESI-MS (*m/z*): 367.3 $[M+H]^+$; Anal. calcd. for $C_{22}H_{23}N_2FO_2$: C, 72.11; H, 6.33; N, 7.64. Found: C, 72.10; H, 6.29; N, 7.62.

Ethyl 2-(2-chloro-6-fluorophenyl)-1-cyclohexyl-1H-benzo[d]imidazole-5-carboxylate (4c): Yield 82%; Mp 104-106°C; Pale yellow crystalline solid; FT IR (ATR, υ_{max}, cm^{-1}): 3000 (Ar-H), 2943, 2858 (C-H), 1710 (C=O), 1618 (C=N), 1570 (C=C), 1298 (C-O), 1249 (C-F), 790 (C-Cl); ^{1}H NMR (400 MHz, $CDCl_3$, δ ppm): 8.49 (d, 1H, Ar-H, *J* = 1.6 Hz), 7.9-7.97 (dd, 1H, Ar-H, *J* = 1.6 and 8.8 Hz), 7.61 (d, 1H, Ar-H, *J* = 8.4 Hz), 7.39-7.45 (m, 1H, Ar-H), 7.31 (d, 1H, Ar-H, *J* = 8.0 Hz), 7.10 (t, 1H, Ar-H, *J* = 8.4 Hz), 4.32-4.37 (q, 2H, -CH_2 of ethyl group, *J* = 6.8 Hz), 3.74-3.81 (m, 1H, cyclohexyl N-CH), 2.05-2.14 (m, 2H, cyclohexyl), 1.83-1.99 (m, 4H, cyclohexyl), 1.67 (m, 1H, cyclohexyl), 1.34 (t, 3H, -CH_3 of ethyl group, *J* = 6.8 Hz), 1.20-1.21 (m, 3H, cyclohexyl); ^{13}C NMR (100 MHz, $CDCl_3$, δ ppm): 167.0, 162.8, 160.3, 146.7, 143.6, 136.5, 136.1, 132.4, 132.3, 125.6, 124.6, 124.0, 122.9, 119.5, 119.3, 114.5, 114.3, 111.8, 60.8, 57.9, 31.4, 25.9, 25.2, 14.4; ESI-MS (*m/z*): 401.3 $[M+H]^+$, 403.3 $[M+2+H]^+$; Anal. calcd. for $C_{22}H_{22}N_2ClFO_2$: C, 65.91; H, 5.53; N, 6.99. Found: C, 65.89; H, 5.51; N, 7.02.

Procedure for the synthesis of benzimidazole carboxylic acids (5a-c)

To a clear solution of **4 a-c** (0.01 mol) in minimum amount of ethanol, catalytic amount of sodium hydroxide in 20 mL of water was added and the solution was refluxed for 3 h. After the completion of the reaction (monitored by TLC, hexane: ethyl acetate (8:2, v/v)), the cooled reaction mixture

was poured onto crushed ice and acidified with dilute HCl. The solid obtained was washed with water, filtered, dried and recrystallized from ethyl alcohol to obtain pure product.

1-Cyclohexyl-2-(4-methoxyphenyl)-1H-benzo[d]imidazole-5-carboxylic acid (5a): Yield 92%; Mp 244-246 °C; Off white solid; FT IR (ATR, υ_{max}, cm^{-1}): 3462 (O-H), 3001 (Ar-H), 2933, 2856 (C-H), 1702 (C=O), 1610 (C=N), 1529 (C=C), 1172 (C-O); ^{1}H NMR (400 MHz, DMSO-d_6, δ ppm): 12.81 (bs, 1H, CO_2H), 8.53 (d, 1H, Ar-H, J = 1.2 Hz), 7.97-7.99 (dd, 1H, Ar-H, J = 1.6 and 8.8 Hz), 7.66 (d, 1H, Ar-H, J = 8.8 Hz), 7.59 (d, 2H, Ar-H, J = 6.8 Hz), 7.07 (d, 2H, Ar-H, J = 6.8 Hz), 4.33-4.39 (m, 1H, N-CH of cyclohexyl), 3.90 (s, 3H, O-CH_3), 2.27-2.36 (m, 2H, cyclohexyl), 1.95-1.99 (m, 4H, cyclohexyl), 1.77-1.79 (m, 1H, cyclohexyl), 1.33-1.38 (m, 3H, cyclohexyl); ^{13}C NMR (100 MHz, DMSO-d_6, δ ppm): 167.3, 160.9, 155.5, 143.4, 137.3, 130.8, 124.3, 123.4, 122.8, 122.2, 114.2, 112.0, 57.1, 55.4, 31.4, 25.9, 25.2; ESI-MS (*m/z*): 351.1 $[M+H]^+$; Anal. calcd. for $C_{21}H_{22}N_2O_3$: C, 71.98; H, 6.33; N, 7.99. Found: C, 71.97; H, 6.30; N, 7.94.

1-Cyclohexyl-2-(4-fluorophenyl)-1H-benzo[d]imidazole-5-carboxylic acid (5b): Yield 94%; Mp 248-250 °C; Off white solid; FT IR (ATR, υ_{max}, cm^{-1}): 3450 (O-H), 3050 (Ar-H), 2927, 2850 (C-H), 1703 (C=O), 1601 (C=N), 1527 (C=C), 1300 (C-O), 1224 (C-F); ^{1}H NMR (400 MHz, DMSO-d_6, δ ppm): 12.80 (bs, 1H, CO_2H), 8.51 (d, 1H, Ar-H, J = 1.2 Hz), 7.99-8.02 (dd, 1H, Ar-H, J = 1.6 and 8.8 Hz), 7.67 (d, 1H, Ar-H, J = 8.8 Hz), 7.62-7.66 (m, 2H, Ar-H), 7.23-7.27 (m, 2H, Ar-H), 4.29-4.35 (m, 1H, cyclohexyl N-CH), 2.27-2.36 (m, 2H, cyclohexyl), 1.95-2.03 (m, 4H, cyclohexyl), 1.76-1.8 (m, 1H, cyclohexyl), 1.35-1.36 (m, 3H, cyclohexyl); ^{13}C NMR (100 MHz, DMSO-d_6, δ ppm): 167.1, 164.9, 162.5, 154.4, 143.3, 137.1, 131.5, 131.4, 126.8, 124.6, 123.7, 122.46, 116.0, 115.9, 112.1, 57.3, 31.5, 25.9, 25.2; ESI-MS (*m/z*): 339.3 $[M+H]^+$; Anal. calcd. for $C_{20}H_{19}N_2FO_2$: C, 70.99; H, 5.66; N, 8.28. Found: C, 70.97; H, 5.62; N, 8.24.

2-(2-Chloro-6-fluorophenyl)-1-cyclohexyl-1H-benzo[d]imidazole-5-carboxylic acid (5c): Yield 96%; Mp 232-234 °C; Off white solid; FT IR (ATR, υ_{max}, cm^{-1}): 3500 (O-H), 2941, 2862 (C-H), 1706 (C=O), 1620 (C=N), 1572 (C=C), 1298 (C-O), 1248 (C-F), 779 (C-Cl); ^{1}H NMR (400 MHz, DMSO-d_6, δ ppm): 12.82 (bs, 1H, CO_2H), 8.30 (s, 1H, Ar-H), 8.01 (d, 1H, Ar-H, J = 12.0 Hz), 7.93 (d, 1H, Ar-H, J = 8.4 Hz), 7.73-7.71 (m, 1H, Ar-H), 7.63 (d, 1H, Ar-H, J = 8.0 Hz), 7.51 (t, 1H, Ar-H, J = 8.0 Hz), 3.84-3.90 (m, 1H, cyclohexyl N-CH), 2.14-2.23 (m, 2H, cyclohexyl), 1.78-1.92 (m, 4H, cyclohexyl), 1.58 (m, 1H, cyclohexyl), 1.23-1.32 (m, 3H, cyclohexyl); ^{13}C NMR (100

MHz, DMSO-d_6, δ ppm): 167.6, 161.9, 159.5, 146.1, 143.0, 136.5, 136.1, 134.7, 132.3, 125.9, 124.7, 123.8, 121.5, 118.4, 118.2, 115.1, 114.9, 112.7, 57.2, 30.7, 25.2, 24.3; ESI-MS (*m/z*): 373.3 $[M+H]^+$, 375.3 $[M+2+H]^+$; Anal. calcd. for $C_{20}H_{18}N_2ClFO_2$: C, 64.43; H, 4.87; N, 7.51. Found: C, 64.41; H, 4.83; N, 7.54.

Procedure for the synthesis of benzimidazole monopeptide esters (6a-l)

To a clear solution of **5a-c** (0.01 mol) in 15 mL of DMF, NMM (0.025 mol, 2.5 equiv.) and TBTU (0.0125 mol, 1.25 equiv.) were added and stirred for an hour at room temperature. To the clear resulting solution, amino acid methyl ester hydrochloride (0.01 mol, 1.0 equiv.) was added and stirred at room temperature for 4 h. After completion of the reaction (monitored by TLC hexane: ethyl acetate (7:3, v/v)), the reaction mass was poured onto crushed ice. The precipitated solid was washed with water, filtered, dried and column purified to obtain the pure product.

Methyl (S)-(1-cyclohexyl-2-(4-methoxyphenyl)-1H-benzo[d]imidazole-5-carbonyl)alaninate (6a): Yield 90%; Mp 134-136 °C; Off white solid; FT IR (ATR, υ_{max}, cm^{-1}): 3078 (Ar-H), 2935 and 2854 (C-H), 1726 (C=O of ester), 1652 (C=O of amide), 1612 (C=N), 1577 (C=C), 1029 (C-O); ^{1}H NMR (400 MHz, $CDCl_3$, δ ppm): 8.65 (d, 1H, amide N-H, *J* = 7.2 Hz), 8.27 (d, 1H, Ar-H, *J* = 1.2 Hz), 7.90 (d, 1H, Ar-H, *J* = 8.4Hz), 7.79-7.82 (dd, 1H, Ar-H, *J* = 1.6 and 7.2 Hz), 7.61 (d, 1H, Ar-H, *J* = 8.8 Hz), 7.15 (d, 1H, Ar-H, *J* = 9.2 Hz), 4.42-4.49 (m, 1H, chiral CH), 4.26-4.32 (m, 1H, N-CH), 3.86 (s, 3H, OCH_3), 3.79 (s, 3H, OCH_3), 2.25-2.33 (m, 2H, cyclohexyl), 1.84-1.92 (m, 4H, cyclohexyl), 1.63-1.66 (m, 1H, cyclohexyl), 1.42-1.44 (d, 3H, CH_3, *J* = 7.2 Hz), 1.23-1.39 (m, 3H, cyclohexyl); ^{13}C NMR (100 MHz, $CDCl_3$, δ ppm): 174.4, 166.4, 160.4, 154.7, 142.8, 135.7, 130.8, 127.5, 122.5, 121.6, 118.7, 114.2, 112.4, 56.7, 55.3, 51.9, 48.2, 30.5, 25.5, 24.4, 16.9; ESI-MS (*m/z*): 436.2 $[M+H]^+$; Anal. calcd. for $C_{25}H_{29}N_3O_4$: C, 68.95; H, 6.71; N, 9.65. Found: C, 68.96; H, 6.70; N, 9.62.

Methyl (S)-(1-cyclohexyl-2-(4-methoxyphenyl)-1H-benzo[d]imidazole-5-carbonyl)valinate (6b): Yield 62%; Mp 68-70 °C; Off white solid; FT IR (ATR, υ_{max}, cm^{-1}): 3409 (NH), 3100 (Ar-H), 2935 and 2850 (C-H), 1722 (C=O of ester), 1650 (C=O of amide), 1612 (C=N), 1581 (C=C), 1029 (C-O); ^{1}H NMR (400 MHz, $CDCl_3$, δ ppm): 8.33 (d, 1H, amide NH, *J* = 8.0 Hz); 8.27 (d,

1H, Ar-H, *J* = 1.2 Hz), 7.89 (d, 1H, Ar-H, *J* = 8.8 Hz), 7.78-7.80 (dd, 1H, Ar-H, *J* = 1.6 and 8.4 Hz), 7.61 (d, 2H, Ar-H, *J* = 8.8 Hz), 7.15 (d, 2H, Ar-H, *J* = 8.8 Hz), 4.26-4.32 (m, 2H, N-CH and chiral CH), 3.86 (s, 3H, OCH_3), 3.79 (s, 3H, OCH_3), 2.19-2.33 (m, 3H, CH and cyclohexyl), 1.84-1.90 (m, 4H, cyclohexyl), 1.63-1.66 (m, 1H, cyclohexyl), 1.23-1.41 (m, 3H, cyclohexyl), 0.97-1.01 (m, 6H, diastereotopic CH_3); ^{13}C NMR (100 MHz, $CDCl_3$, δ ppm): 174.3, 166.9, 160.4, 154.6, 142.7, 135.7, 130.8, 127.8, 122.5, 121.7, 118.8, 114.2, 112.4, 58.6, 56.7, 55.3, 51.8, 30.5, 29.6, 25.5, 24.4, 19.4, 18.8; ESI-MS (*m/z*): 464.4 $[M+H]^+$; Anal. calcd. for $C_{27}H_{33}N_3O_4$: C, 69.96; H, 7.18; N, 9.06. Found: C, 69.94; H, 7.15; N, 9.03.

Methyl (S)-(1-cyclohexyl-2-(4-methoxyphenyl)-1H-benzo[d]imidazole-5-carbonyl)leucinate (6c): Yield 75%; Mp: 82-84 °C; Off white solid; FT IR (ATR, υ_{max}, cm^{-1}): 3074 (Ar-H), 2935 and 2862 (C-H), 1726 (C=O of ester), 1650 (C=O of amide), 1612 (C=N), 1577 (C=C), 1029 (C-O); ^{1}H NMR (400 MHz, $CDCl_3$, δ ppm): 8.33 (d, 1H, amide NH, *J* = 6.8 Hz), 8.23 (s, 1H, Ar-H), 7.88 (d, 1H, Ar-H, *J* = 8.4 Hz), 7.78 (d, 1H, Ar-H, *J* = 8.4 Hz), 7.60 (d, 1H, Ar-H, *J* = 8.4 Hz), 7.14 (d, 1H, Ar-H, *J* = 8.8 Hz), 4.37-4.40 (m, 1H, chiral CH), 4.25-4.31 (m, 1H, C-NH), 3.86 (s, 3H, OCH_3), 3.79 (s, 3H, OCH_3), 2.24-2.33 (m, 2H, cyclohexyl), 1.83-1.90 (m, 4H, cyclohexyl), 1.62-1.76 (m, 4H, isobutyl CH, CH_2 and cyclohexyl), 1.24-1.41 (m, 3H, cyclohexyl), 0.89-0.92 (m, 6H, diastereotopic CH_3); ^{13}C NMR (100 MHz, $CDCl_3$, δ ppm): 174.4, 166.4, 160.4, 154.6, 142.8, 135.6, 130.8, 128.0, 122.5, 121.5, 118.6, 114.2, 112.4, 56.6, 55.3, 52.2, 30.5, 29.6, 25.5, 24.6, 23.0, 21.6, 18.9; ESI-MS (*m/z*): 478.4 $[M+H]^+$; Anal. calcd. for $C_{28}H_{35}N_3O_4$: C, 70.42; H, 7.39; N, 8.80. Found: C, 70.40; H, 7.35; N, 8.81.

Methyl (S)-(1-cyclohexyl-2-(4-methoxyphenyl)-1H-benzo[d]imidazole-5-carbonyl)tryptophanate (6d): Yield 99%, Mp: 86-88 °C; Off white to pale brown solid; FT IR (ATR, υ_{max}, cm^{-1}): 3055 (Ar-H), 2933 and 2856 (C-H), 1728 (C=O of ester), 1643 (C=O of amide), 1612 (C=N), 1577 (C=C), 1178 (C-O); ^{1}H NMR (400 MHz, $CDCl_3$, δ ppm): 10.81 (s, 1H, indole NH), 8.62 (d, 1H, amide NH, *J* = 7.6 Hz), 8.20 (d, 1H, Ar-H, *J* = 1.6 Hz), 7.88 (d, 1H, Ar-H, *J* = 8.4 Hz), 7.72-7.75 (dd, 1H, Ar-H, *J* = 8.4 and 1.6 Hz), 7.59-7.63 (m, 3H, Ar-H), 7.32 (d, 1H, Ar-H, *J* = 8.0 Hz), 7.23 (d, 1H, Ar-H, *J* = 2.0 Hz), 7.15 (d, 2H, Ar-H, *J* = 8.8 Hz), 7.04-7.08 (m, 1H, Ar-H), 6.97-7.01 (m, 1H, Ar-H), 4.66-4.72 (m, 1H, chiral CH), 4.25-4.31 (m, 1H, C-NH), 3.86 (s, 3H, OCH_3), 3.79 (s, 3H, OCH_3), 2.23-2.29 (m, 2H, cyclohexyl), 1.83-1.89 (m, 4H, cyclohexyl), 1.62-1.65 (m, 1H, cyclohexyl), 1.25-1.41 (m, 3H, cyclohexyl); ^{13}C NMR (100 MHz, $CDCl_3$, δ ppm): 173.7, 166.6,

160.4, 154.6, 142.6, 136.1, 135.6, 130.9, 127.6, 127.1, 125.76, 123.6, 121.6, 120.9, 118.5, 118.4, 118.1, 114.2, 112.5, 111.4, 110.5, 56.7, 55.3, 53.7, 52.4, 30.5, 26.6, 25.5, 24.3; ESI-MS (*m/z*): 551.3 $[M+H]^+$; Anal. calcd. for $C_{33}H_{34}N_4O_4$: C, 71.98; H, 6.22; N, 10.17. Found: C, 71.95; H, 6.20; N, 10.13

Methyl (S)-(1-cyclohexyl-2-(4-fluorophenyl)-1H-benzo[d]imidazole-5-carbonyl)alaninate (6e): Yield 86%; Mp 128-130 °C; Off white solid; IR (ATR, υ_{max}, cm^{-1}): 3071 (Ar-H), 2932 and 2861 (C-H), 1730 (C=O of ester), 1653 (C=O of amide), 1614 (C=N), 1578 (C=C), 1265 (C-O), 1230 (C-F); ^1H NMR (400 MHz, $CDCl_3$, δ ppm): 8.63 (d, 1H, amide N-H, J = 7.2 Hz), 8.29 (s, 1H, Ar-H), 7.93 (d, 1H, Ar-H, J = 8.8 Hz), 7.83 (d, 1H, Ar-H, J = 8.8 Hz), 7.71-7.75 (m, 2H, Ar-H), 7.42-7.46 (m, 2H, Ar-H), 4.41-4.48 (m, 1H, chiral CH), 4.20-4.26 (m, 1H, N-CH), 3.79 (s, 3H, OCH_3), 2.24-2.32 (m, 2H, cyclohexyl), 1.83-1.93 (m, 4H, cyclohexyl), 1.63-1.66 (m, 1H, cyclohexyl), 1.42-1.44 (d, 3H, CH_3, J = 7.2 Hz), 1.23-1.38 (m, 3H, cyclohexyl); ^{13}C NMR (100 MHz, $CDCl_3$, δ ppm): 174.5, 166.3, 164.2, 161.7, 153.7, 142.7, 135.7, 131.8, 131.7, 127.7, 126.9, 121.9, 118.9, 115.9, 115.7, 112.6, 56.8, 52.1, 48.4, 30.5, 25.4, 24.3, 17.1; ESI-MS (*m/z*): 424.4 $[M+H]^+$; Anal. calcd. for $C_{24}H_{26}N_3FO_3$: C, 68.07; H, 6.19; N, 9.92. Found: C, 68.02; H, 6.15; N, 9.91.

Methyl (S)-(1-cyclohexyl-2-(4-fluorophenyl)-1H-benzo[d]imidazole-5-carbonyl)valinate (6f): Yield 92%; 118-120 °C; Off white solid; IR (ATR, υ_{max}, cm^{-1}): 3407 (N-H), 3074 (Ar-H), 2935 and 2864 (C-H), 1721 (C=O of ester), 1654 (C=O of amide), 1614 (C=N), 1581 (C=C), 1265 (C-O), 1232 (C-F); ^1H NMR (400 MHz, $CDCl_3$, δ ppm): 8.52 (d, 1H, amide N-H, J = 7.6 Hz), 8.20 (d, 1H, Ar-H, J = 1.2 Hz), 7.90 (d, 1H, Ar-H, J = 8.8 Hz), 7.74-7.76 (m, 1H, Ar-H), 7.71-7.73 (m, 2H, Ar-H), 7.42-7.46 (m, 2H, Ar-H), 4.29-4.32 (m, 1H, chiral CH), 4.26-4.28 (m, 1H, N-CH), 3.79 (s, 3H, OCH_3), 2.25-2.33 (m, 2H, cyclohexyl), 2.20-2.25 (m, 1H, C-H of isopropyl), 1.84-1.90 (m, 4H, cyclohexyl), 1.63-1.66 (m, 1H, cyclohexyl), 1.24-1.41 (m, 3H, cyclohexyl), 0.97-1.01 (m, 6H, diastereotopic CH_3); ^{13}C NMR (100 MHz, $CDCl_3$, δ ppm): 174.4, 166.9, 164.2, 161.7, 154.6, 142.8, 135.7, 131.8, 131.7, 127.5, 122.5, 121.6, 118.7, 115.9, 115.7, 112.4, 58.6, 56.3, 52.3, 30.5, 29.6, 25.5, 24.4, 19.4, 18.8; ESI-MS (*m/z*): 452.4 $[M+H]^+$; Anal. calcd. for $C_{26}H_{30}N_3FO_3$: C, 69.16; H, 6.70; N, 9.31. Found: C, 69.13; H, 6.69; N, 9.32.

Methyl (S)-(1-cyclohexyl-2-(4-fluorophenyl)-1H-benzo[d]imidazole-5-carbonyl)leucinate (6g): Yield 96%, 102-104 °C; Off white solid; IR (ATR, υ_{max}, cm^{-1}): 3409 (N-H), 3071 (Ar-H), 2934

and 2865 (C-H), 1717 (C=O of ester), 1654 (C=O of amide), 1614 (C=N), 1579 (C=C), 1265 (C-O), 1231 (C-F); ^{1}H NMR (400 MHz, $CDCl_3$, δ ppm): 8.59 (d, 1H, amide N-H, *J* = 7.6 Hz), 8.3 (s, 1H, Ar-H), 7.93 (d, 1H, Ar-H, *J* = 8.4 Hz), 7.84 (d, 2H, Ar-H, *J* = 8.4 Hz), 7.72-7.75 (m, 2H, Ar-H), 7.42-7.46 (m, 2H, Ar-H), 4.47-4.52 (m, 1H, chiral CH), 4.20-4.26 (m, 1H, N-CH), 3.79 (s, 3H, OCH_3), 2.24-2.32 (m, 2H, cyclohexyl), 1.59-1.92 (m, 8H, cyclohexyl, isobutyl CH and diastereotopic CH_2), 1.23-1.41 (m, 3H, cyclohexyl), 0.95 (d, 3H, diastereotopic CH_3, *J* = 6.4 Hz) 0.91 (d, 3H, diastereotopic CH_3, *J* = 6.4 Hz); ^{13}C NMR (100 MHz, $CDCl_3$, δ ppm): 174.4, 166.7, 164.2, 161.7, 153.7, 142.6, 135.6, 131.8, 131.7, 127.7, 126.8, 121.9, 118.9, 115.9, 115.7, 112.6, 56.8, 52.1, 50.9, 30.5, 25.4, 24.6, 24.3, 22.9, 21.2; ESI-MS (*m/z*): 466.4 $[M+H]^+$; Anal. calcd. for $C_{27}H_{32}N_3FO_3$: C, 69.66; H, 6.93; N, 9.03. Found: C, 69.64; H, 6.91; N, 9.04.

Methyl (S)-(1-cyclohexyl-2-(4-fluorophenyl)-1H-benzo[d]imidazole-5-carbonyl)- tryptophanate (6h): Yield 96%; Mp 78-80 °C; Off white solid; FT IR (ATR, υ_{max}, cm^{-1}): 3409 (N-H), 3056 (Ar-H), 2933 and 2858 (C-H), 1720 (C=O of ester), 1641 (C=O of amide), 1614 (C=N), 1527 (C=C), 1296 (C-O), 1230 (C-F); ^{1}H NMR (400 MHz, $CDCl_3$, δ ppm): 10.79 (s, 1H, indole-NH), 8.52 (d, 1H, amide-NH, *J* = 7.6 Hz), 8.2 (d, 1H, Ar-H, *J* = 1.2 Hz), 7.90 (d, 1H, Ar-H, *J* = 8.8 Hz), 7.71-7.76 (m, 3H, Ar-H), 7.62 (d, 1H, Ar-H, *J* = 8.0 Hz), 7.44 (m, 2H, Ar-H, *J* = 8.8 Hz), 7.32 (d, 1H, Ar-H, *J* = 8.0 Hz), 7.22 (d, 1H, Ar-H, *J* = 2.0 Hz), 7.03-7.07 (m, 1H, Ar-H); 6.95-6.99 (m, 1H, Ar-H); 4.63-4.68 (m, 1H, chiral C-H), 4.19-4.25 (m, 1H, -NC-H), 3.79 (s, 3H, OCH_3), 3.33-3.38 (dd, 1H, indole CH_2, *J* = 4.2 and 14.6 Hz), 3.23-3.29 (dd, 1H, indole CH_2, *J* = 9.2 and 14.4 Hz), 2.22-2.31 (m, 2H, cyclohexyl), 1.82-1.92 (m, 4H, cyclohexyl), 1.62-1.65 (m, 1H, cyclohexyl), 1.26-1.40 (m, 3H, cyclohexyl); ^{13}C NMR (100 MHz, $CDCl_3$, δ ppm): 173.8, 166.3, 164.2, 161.7, 153.7, 142.6, 136.0, 135.6, 131.8, 131.7, 128.0, 127.3, 126.9, 125.9, 123.5, 121.7, 120.8, 118.7, 118.2, 115.8, 115.7, 112.6, 111.3, 110.7, 56.8, 54.1, 51.9, 30.5, 26.8, 25.4, 24.3; ESI-MS (*m/z*): 539.22 $[M+H]^+$; Anal. calcd. for $C_{32}H_{31}N_4FO_3$: C, 71.36; H, 5.80; N, 10.40. Found: C, 71.37; H, 5.78; N, 10.36.

Methyl (S)-(2-(2-chloro-6-fluorophenyl)-1-cyclohexyl-1H-benzo[d]imidazole-5-carbonyl)-alaninate (6i): Yield 88%; Mp 104-106 °C; Off white solid; IR (ATR, υ_{max}, cm^{-1}): 2928 and 2863 (C-H), 1738 (C=O of ester), 1642 (C=O of amide), 1614 (C=N), 1532 (C=C), 1159 (C-O), 781 (C-C-Cl); ^{1}H NMR (400 MHz, $CDCl_3$, δ ppm): 8.27 (s, 1H, Ar-H), 7.86 (d, 1H, Ar-H, *J* = 8.0 Hz), 7.70 (d, 1H, Ar-H, *J* = 8.0 Hz), 7.47-7.51 (m, 1H, Ar-H), 7.37-7.39 (m, 1H, Ar-H), 7.17 (t, 1H,

Ar-H, *J* = 8.0 Hz), 6.90 (bs, 1H, amide N-H), 4.83-4.86 (m, 1H, chiral CH), 3.83-3.87 (m, 1H, N-CH), 3.79 (s, 3H, OCH_3), 1.91-2.18 (m, 6H, cyclohexyl), 1.55 (d, 3H, CH_3, *J* = 8.0 Hz), 1.27-1.31 (m, 4H, cyclohexyl); ^{13}C NMR (100 MHz, $CDCl_3$, δ ppm): 173.7, 167.2, 162.7, 160.2, 146.7, 143.6, 136.1, 135.7, 132.4, 132.3, 128.2, 125.6, 122.3, 119.4, 114.5, 114.3, 112.4, 58.0, 52.5, 48.6, 31.5, 25.9, 25.1, 18.6; ESI-MS (*m/z*): 458.2 $[M+H]^+$, 460.2 $[M+2+H]^+$; Anal. calcd. for $C_{24}H_{25}N_3ClFO_3$: C, 62.95; H, 5.50; N, 9.18. Found: C, 62.92; H, 5.48; N, 9.15.

Methyl (S)-(2-(2-chloro-6-fluorophenyl)-1-cyclohexyl-1H-benzo[d]imidazole-5-carbonyl)-valinate (6j): Yield 86%; Mp 58-60 °C; Off white solid; IR (ATR, υ_{max}, cm^{-1}): 3362 (O-H), 3073 (Ar-H), 2947 and 2861 (C-H), 1724 (C=O of ester), 1644 (C=O of amide), 1621 (C=N), 1574 (C=C), 1297 (C-O), 1246 (C-F); ^1H NMR (400 MHz, $CDCl_3$, δ ppm): 8.61 (d, 1H, amide N-H, *J* = 8.0 Hz), 8.34 (s, 1H, Ar-H), 7.97 (d, 1H, Ar-H, *J* = 8.4 Hz), 7.87 (d, 1H, Ar-H, *J* = 8.8 Hz), 7.71-7.77 (m, 1H, Ar-H), 7.62 (m, 1H, Ar-H), 7.49-7.54 (m, 1H, Ar-H), 4.29-4.32 (m, 1H, chiral CH), 4.26-4.28 (m, 1H, N-CH), 3.79 (s, 3H, OCH_3), 2.25-2.33 (m, 2H, cyclohexyl), 2.20-2.25 (m, 1H, C-H of isopropyl), 1.84-1.90 (m, 4H, cyclohexyl), 1.63-1.66 (m, 1H, cyclohexyl), 1.24-1.41 (m, 3H, cyclohexyl), 0.97-1.01 (m, 6H, diastereotopic CH_3); ^{13}C NMR (100 MHz, $CDCl_3$, δ ppm): 174.4, 166.4, 162.9, 160.5, 146.8, 143.7, 136.5, 132.3, 125.5, 124.5, 122.9, 114.4, 114.2, 111.9, 58.7, 56.6, 52.4, 30.5, 29.6, 25.5, 24.4, 19.4, 18.9; ESI-MS (*m/z*): 486.4 $[M+H]^+$, 488.4 $[M+2+H]^+$; Anal. calcd. for $C_{26}H_{29}N_3ClFO_3$: C, 64.26; H, 6.02; N, 8.65. Found: C, 64.20; H, 5.99; N, 8.61.

Methyl (S)-(2-(2-chloro-6-fluorophenyl)-1-cyclohexyl-1H-benzo[d]imidazole-5-carbonyl)-leucinate (6k): Yield 96%; Mp 54-56 °C; Off white solid; IR (ATR, υ_{max}, cm^{-1}): 3355 (O-H), 3080 (Ar-H), 2948 and 2864 (C-H), 1722 (C=O of ester), 1643 (C=O of amide), 1620 (C=N), 1571 (C=C), 1299 (C-O), 1249 (C-F); ^1H NMR (400 MHz, $CDCl_3$, δ ppm): 12.51 (s, 1H, CO_2H), 8.61 (d, 1H, amide N-H, *J* = 8.0 Hz), 8.34 (s, 1H, Ar-H), 7.97 (d, 1H, Ar-H, *J* = 8.4 Hz), 7.87 (d, 1H, Ar-H, *J* = 8.8 Hz), 7.71-7.77 (m, 1H, Ar-H), 7.62 (m, 1H, Ar-H), 7.49-7.54 (m, 1H, Ar-H), 4.47-4.51 (m, 1H, chiral C-H), 3.84-3.90 (m, 1H, N-CH), 3.79 (s, 3H, OCH_3), 2.12-2.21 (m, 2H, cyclohexyl), 1.60-1.84 (m, 8H, cyclohexyl, isobutyl CH and diastereotopic CH_2), 1.24-1.29 (m, 3H, cyclohexyl), 0.94 (d, 3H, diastereotopic CH_3, *J* = 6.4 Hz), 0.90 (d, 3H, diastereotopic CH_3, *J* = 6.4 Hz); ^{13}C NMR (100 MHz, $CDCl_3$, δ ppm): 174.4, 166.4, 162.8, 160.5, 146.8, 143.7, 136.5, 132.3, 125.5, 124.5, 124.0, 122.9, 114.5, 114.3, 111.9, 56.6, 50.9, 52.1, 30.5, 25.5, 24.6, 24.3, 23.1,

21.6; ESI-MS (*m/z*): 500.2 $[M+H]^+$, 502.2 $[M+2+H]^+$; Anal. calcd. for $C_{27}H_{31}N_3ClFO_3$: C, 64.86; H, 6.25; N, 8.40. Found: C, 64.85; H, 6.23; N, 8.42.

Methyl (S)-(2-(2-chloro-6-fluorophenyl)-1-cyclohexyl-1H-benzo[d]imidazole-5-carbonyl)-tryptophanate (6l): Yield 97%; Mp 84-86 °C; Off white solid; FT IR (ATR, υ_{max}, cm^{-1}): 3409 (N-H), 3056 (Ar-H), 2937 and 2858 (C-H), 1724 (C=O of ester), 1641 (C=O of amide), 1620 (C=N), 1573 (C=C), 1299 (C-O), 1251 (C-F); ^1H NMR (400 MHz, $CDCl_3$, δ ppm): 10.80 (s, 1H, indole-NH), 8.67 (d, 1H, amide N-H, J = 7.6 Hz), 8.27 (s, 1H, Ar-H), 7.95 (d, 1H, Ar-H, J = 8.4 Hz), 7.71-7.80 (m, 2H, Ar-H), 7.60-7.63 (m, 2H, Ar-H), 7.49-7.53 (m, 1H, Ar-H), 7.32 (d, 1H, Ar-H, J = 8.0 Hz), 7.23 (s, 1H, Ar-H), 7.04-7.08 (m, 1H, Ar-H), 6.98-7.01 (m, 1H, Ar-H), 4.67-4.72 (m, 1H, chiral C-H), 3.83-3.89 (m, 1H, N-CH), 3.79 (s, 3H, OCH_3), 3.22-3.28 (m, 2H, indolyl CH_2), 2.07-2.18 (m, 2H, cyclohexyl), 1.79-1.90 (m, 4H, cyclohexyl), 1.59-1.61 (m, 1H, cyclohexyl), 1.17-1.28 (m, 3H, cyclohexyl); ^{13}C NMR (100 MHz, $CDCl_3$, δ ppm): 173.6, 166.6, 161.9, 159.5, 145.8, 142.8, 136.2, 135.1, 134.8, 133.6, 128.1, 127.2, 125.9, 123.6, 122.5, 120.9, 119.2, 118.4, 118.1, 114.9, 112.3, 111.5, 110.5, 57.2, 53.9, 52.2, 30.8, 26.6, 25.3, 24.3; ESI-MS (*m/z*): 573.3 $[M+H]^+$, 575.3 $[M+2+H]^+$; Anal. calcd. for $C_{32}H_{30}N_4ClFO_3$: C, 67.07; H, 5.28; N, 9.78. Found: C, 67.05; H, 5.27; N, 9.76.

Procedure for the synthesis of benzimidazole monopeptides (7a-l)

To a stirred clear solution of **6a-l** (0.01 mol) in 20 mL of THF:water (2:1) mixture, $LiOH.H_2O$ (0.015 mol, 1.5 equiv.) was added at 0 °C. The stirring was continued at this temperature for 4 h. After completion of the reaction (monitored by TLC, hexane: ethyl acetate (4:6, v/v)), the reaction mass was quenched to crushed ice, acidified with dilute HCl. The resulting solid was washed with water and dried. The solid was subjected to column chromatography to obtain pure benzimidazole monopeptides.

(S)-(1-Cyclohexyl-2-(4-methoxyphenyl)-1H-benzo[d]imidazole-5-carbonyl)alanine (7a): Yield 71%; Mp 278-280°C; Off white solid; FT IR (ATR, υ_{max}, cm^{-1}): 3406 (O-H), 3078 (Ar-H), 2935 and 2854 (C-H), 1716 (C=O of acid), 1654 (C=O of amide), 1612 (C=N), 1577 (C=C), 1029 (C-O); ^1H NMR (400 MHz, DMSO-d_6, δ ppm): 12.44 (s, 1H, CO_2H), 8.65 (d, 1H, amide N-H, J = 7.2

Hz), 8.27 (d, 1H, Ar-H, *J* = 1.2 Hz), 7.90 (d, 1H, Ar-H, *J* = 8.4Hz), 7.79-7.82 (dd, 1H, Ar-H, *J* = 1.6 and 7.2 Hz), 7.61 (d, 1H, Ar-H, *J* = 8.8 Hz), 7.15 (d, 1H, Ar-H, *J* = 9.2 Hz), 4.42-4.49 (m, 1H, chiral CH), 4.26-4.32 (m, 1H, N-CH), 3.86 (s, 3H, OCH_3), 2.25-2.33 (m, 2H, cyclohexyl), 1.84-1.92 (m, 4H, cyclohexyl), 1.63-1.66 (m, 1H, cyclohexyl), 1.42-1.44 (d, 3H, CH_3, *J* = 7.2 Hz), 1.23-1.39 (m, 3H, cyclohexyl); ^{13}C NMR (100 MHz, DMSO-d_6, δ ppm): 174.4, 166.4, 160.4, 154.7, 142.8, 135.7, 130.8, 127.5, 122.5, 121.6, 118.7, 114.2, 112.4, 56.7, 55.3, 48.2, 30.5, 25.5, 24.4, 16.9; ESI-MS (*m/z*): 422.4 $[M+H]^+$; Anal. calcd. for $C_{24}H_{27}N_3O_4$: C, 68.39; H, 6.46; N, 9.97. Found: C, 68.35; H, 6.47; N, 9.94.

(S)-(1-Cyclohexyl-2-(4-methoxyphenyl)-1H-benzo[d]imidazole-5-carbonyl)valine (7b): Yield 50%; Mp 194-196°C; Off white solid; FT IR (ATR, υ_{max}, cm^{-1}): 3409 (O-H), 3379 and 3409 (NH), 3100 (Ar-H), 2935 and 2850 (C-H), 1712 (C=O of acid), 1650 (C=O of amide), 1612 (C=N), 1581 (C=C), 1029 (C-O); ^{1}H NMR (400 MHz, DMSO-d_6, δ ppm): 8.33 (d, 1H, amide NH, *J* = 8.0 Hz); 8.27 (d, 1H, Ar-H, *J* = 1.2 Hz), 7.89 (d, 1H, Ar-H, *J* = 8.8 Hz), 7.78-7.80 (dd, 1H, Ar-H, *J* = 1.6 and 8.4 Hz), 7.61 (d, 2H, Ar-H, *J* = 8.8 Hz), 7.15 (d, 2H, Ar-H, *J* = 8.8 Hz), 4.26-4.32 (m, 2H, N-CH and chiral CH), 3.86 (s, 3H, OCH_3), 2.19-2.33 (m, 3H, CH and cyclohexyl), 1.84-1.90 (m, 4H, cyclohexyl), 1.63-1.66 (m, 1H, cyclohexyl), 1.23-1.41 (m, 3H, cyclohexyl), 0.97-1.01 (m, 6H, diastereotopic CH_3); ^{13}C NMR (100 MHz, DMSO-d_6, δ ppm): 174.3, 166.9, 160.4, 154.6, 142.7, 135.7, 130.8, 127.8, 122.5, 121.7, 118.8, 114.2, 112.4, 58.6, 56.7, 55.3, 30.5, 29.6, 25.5, 24.4, 19.4, 18.8; ESI-MS (*m/z*): 450.4 $[M+H]^+$; Anal. calcd. for $C_{26}H_{31}N_3O_4$: C, 69.47; H, 6.95; N, 9.35. Found: C, 69.45; H, 6.92; N, 9.37.

(S)-(1-Cyclohexyl-2-(4-methoxyphenyl)-1H-benzo[d]imidazole-5-carbonyl)leucine (7c): Yield 66%; Mp: 224-226°C; Off white solid; FT IR (ATR, υ_{max}, cm^{-1}): 3413 (O-H), 3074 (Ar-H), 2935 and 2862 (C-H), 1712 (C=O of acid), 1650 (C=O of amide), 1612 (C=N), 1577 (C=C), 1029 (C-O); ^{1}H NMR (400 MHz, DMSO-d_6, δ ppm): 8.33 (d, 1H, amide NH, *J* = 6.8 Hz), 8.23 (s, 1H, Ar-H), 7.88 (d, 1H, Ar-H, *J* = 8.4 Hz), 7.78 (d, 1H, Ar-H, *J* = 8.4 Hz), 7.60 (d, 1H, Ar-H, *J* = 8.4 Hz), 7.14 (d, 1H, Ar-H, *J* = 8.8 Hz), 4.37-4.40 (m, 1H, chiral CH), 4.25-4.31 (m, 1H, C-NH), 3.86 (s, 3H, OCH_3), 2.24-2.33 (m, 2H, cyclohexyl), 1.83-1.90 (m, 4H, cyclohexyl), 1.62-1.76 (m, 4H, isobutyl CH, CH_2 and cyclohexyl), 1.24-1.41 (m, 3H, cyclohexyl), 0.89-0.92 (m, 6H, diastereotopic CH_3); ^{13}C NMR (100 MHz, DMSO-d_6, δ ppm): 174.4, 166.4, 160.4, 154.6, 142.8, 135.6, 130.8, 128.0, 122.5, 121.5, 118.6, 114.2, 112.4, 56.6, 55.3, 30.5, 29.6, 25.5, 24.6, 23.0, 21.6,

18.9; ESI-MS (*m/z*): 464.4 $[M+H]^+$; Anal. calcd. for $C_{27}H_{33}N_3O_4$: C, 69.95; H, 7.18; N, 9.06. Found: C, 69.96; H, 7.15; N, 9.04.

(S)-(1-Cyclohexyl-2-(4-methoxyphenyl)-1H-benzo[d]imidazole-5-carbonyl)tryptophan (7d): Yield 99%, Mp: 172-174°C; Off white to pale brown solid; FT IR (ATR, υ_{max}, cm^{-1}): 3406 (O-H), 3055 (Ar-H), 2933 and 2856 (C-H), 1720 (C=O of acid), 1643 (C=O of amide), 1612 (C=N), 1577 (C=C), 1178 (C-O); ^1H NMR (400 MHz, DMSO-d_6, δ ppm): 10.81 (s, 1H, indole NH), 8.62 (d, 1H, amide NH, J = 7.6 Hz), 8.20 (d, 1H, Ar-H, J = 1.6 Hz), 7.88 (d, 1H, Ar-H, J = 8.4 Hz), 7.72-7.75 (dd, 1H, Ar-H, J = 8.4 and 1.6 Hz), 7.59-7.63 (m, 3H, Ar-H), 7.32 (d, 1H, Ar-H, J = 8.0 Hz), 7.23 (d, 1H, Ar-H, J = 2.0 Hz), 7.15 (d, 2H, Ar-H, J = 8.8 Hz), 7.04-7.08 (m, 1H, Ar-H), 6.97-7.01 (m, 1H, Ar-H), 4.66-4.72 (m, 1H, chiral CH), 4.25-4.31 (m, 1H, C-NH), 3.86 (s, 3H, OCH_3), 2.23-2.29 (m, 2H, cyclohexyl), 1.83-1.89 (m, 4H, cyclohexyl), 1.62-1.65 (m, 1H, cyclohexyl), 1.25-1.41 (m, 3H, cyclohexyl); ^{13}C NMR (100 MHz, DMSO-d_6, δ ppm): 173.7, 166.6, 160.4, 154.6, 142.6, 136.1, 135.6, 130.9, 127.6, 127.1, 125.76, 123.6, 121.6, 120.9, 118.5, 118.4, 118.1, 114.2, 112.5, 111.4, 110.5, 56.7, 55.3, 53.7, 30.5, 26.6, 25.5, 24.3; ESI-MS (*m/z*): 537.5 $[M+H]^+$; Anal. calcd. for $C_{32}H_{32}N_4O_4$: C, 71.62; H, 6.01; N, 10.44. Found: C, 71.59; H, 6.02; N, 10.41.

(S)-(1-Cyclohexyl-2-(4-fluorophenyl)-1H-benzo[d]imidazole-5-carbonyl)alanine (7e): Yield 75%; Mp 272-274°C; Off white solid; IR (ATR, υ_{max}, cm^{-1}): 3411 (O-H), 3071 (Ar-H), 2932 and 2861 (C-H), 1706 (C=O of acid), 1653 (C=O of amide), 1614 (C=N), 1578 (C=C), 1265 (C-O), 1230 (C-F); ^1H NMR (400 MHz, DMSO-d_6, δ ppm): 8.63 (d, 1H, amide N-H, J = 7.2 Hz), 8.29 (s, 1H, Ar-H), 7.93 (d, 1H, Ar-H, J = 8.8 Hz), 7.83 (d, 1H, Ar-H, J = 8.8 Hz), 7.71-7.75 (m, 2H, Ar-H), 7.42-7.46 (m, 2H, Ar-H), 4.41-4.48 (m, 1H, chiral CH), 4.20-4.26 (m, 1H, N-CH), 2.24-2.32 (m, 2H, cyclohexyl), 1.83-1.93 (m, 4H, cyclohexyl), 1.63-1.66 (m, 1H, cyclohexyl), 1.42-1.44 (d, 3H, CH_3, J = 7.2 Hz), 1.23-1.38 (m, 3H, cyclohexyl); ^{13}C NMR (100 MHz, DMSO-d_6, δ ppm): 174.5, 166.3, 164.2, 161.7, 153.7, 142.7, 135.7, 131.8, 131.7, 127.7, 126.9, 121.9, 118.9, 115.9, 115.7, 112.6, 56.8, 48.4, 30.5, 25.4, 24.3, 17.1; ESI-MS (*m/z*): 410.4 $[M+H]^+$; Anal. calcd. for $C_{23}H_{24}N_3FO_3$: C, 67.47; H, 5.91; N, 10.26. Found: C, 67.43; H, 5.88; N, 10.27.

(S)-(1-Cyclohexyl-2-(4-fluorophenyl)-1H-benzo[d]imidazole-5-carbonyl)valine (7f): Yield 89%; 262-264°C; Off white solid; IR (ATR, υ_{max}, cm^{-1}): 3407 (O-H), 3074 (Ar-H), 2935 and 2864 (C-H), 1706 (C=O of acid), 1654 (C=O of amide), 1614 (C=N), 1581 (C=C), 1265 (C-O), 1232

(C-F); ^{1}H NMR (400 MHz, DMSO-d_6, δ ppm): 8.52 (d, 1H, amide N-H, J = 7.6 Hz), 8.20 (d, 1H, Ar-H, J = 1.2 Hz), 7.90 (d, 1H, Ar-H, J = 8.8 Hz), 7.74-7.76 (m, 1H, Ar-H), 7.71-7.73 (m, 2H, Ar-H), 7.42-7.46 (m, 2H, Ar-H), 4.29-4.32 (m, 1H, chiral CH), 4.26-4.28 (m, 1H, N-CH), 2.25-2.33 (m, 2H, cyclohexyl), 2.20-2.25 (m, 1H, C-H of isopropyl), 1.84-1.90 (m, 4H, cyclohexyl), 1.63-1.66 (m, 1H, cyclohexyl), 1.24-1.41 (m, 3H, cyclohexyl), 0.97-1.01 (m, 6H, diastereotopic CH_3); ^{13}C NMR (100 MHz, DMSO-d_6, δ ppm): 174.4, 166.9, 164.2, 161.7, 154.6, 142.8, 135.7, 131.8, 131.7, 130.8, 127.5, 121.6, 118.7, 115.9, 115.7, 112.4, 58.6, 56.3, 30.5, 29.6, 25.5, 24.4, 19.4, 18.8; ESI-MS (*m/z*): 438.4 $[M+H]^+$; Anal. calcd. for $C_{25}H_{28}N_3FO_3$: C, 68.63; H, 6.45; N, 9.60. Found: C, 68.65; H, 6.44; N, 9.62.

(S)-(1-Cyclohexyl-2-(4-fluorophenyl)-1H-benzo[d]imidazole-5-carbonyl)leucine (7g): Yield 90%, 244-248°C; Off white solid; IR (ATR, υ_{max}, cm^{-1}): 3409 (O-H), 3071 (Ar-H), 2934 and 2865 (C-H), 1707 (C=O of acid), 1654 (C=O of amide), 1614 (C=N), 1579 (C=C), 1265 (C-O), 1231 (C-F); ^{1}H NMR (400 MHz, DMSO-d_6, δ ppm): 8.59 (d, 1H, amide N-H, J = 7.6 Hz), 8.3 (s, 1H, Ar-H), 7.93 (d, 1H, Ar-H, J = 8.4 Hz), 7.84 (d, 1H, Ar-H, J = 8.4 Hz), 7.72-7.75 (m, 2H, Ar-H), 7.42-7.46 (m, 2H, Ar-H), 4.47-4.52 (m, 1H, chiral CH), 4.20-4.26 (m, 1H, N-CH), 2.24-2.32 (m, 2H, cyclohexyl), 1.59-1.92 (m, 8H, cyclohexyl, isobutyl CH and diastereotopic CH_2), 1.23-1.41 (m, 3H, cyclohexyl), 0.95 (d, 3H, diastereotopic CH_3, J = 6.4 Hz) 0.91 (d, 3H, diastereotopic CH_3, J = 6.4 Hz); ^{13}C NMR (100 MHz, DMSO-d_6, δ ppm): 174.4, 166.7, 164.2, 161.7, 153.7, 142.6, 135.6, 131.8, 131.7, 127.7, 126.8, 121.9, 118.9, 115.9, 115.8, 112.6, 56.8, 50.9, 30.5, 25.4, 24.6, 24.3, 22.9, 21.2; ESI-MS (*m/z*): 450.4 $[M-H]^-$; Anal. calcd. for $C_{26}H_{30}N_3FO_3$: C, 69.16; H, 6.70; N, 9.31. Found: C, 69.14; H, 6.73; N, 9.34.

(S)-(1-Cyclohexyl-2-(4-fluorophenyl)-1H-benzo[d]imidazole-5-carbonyl)tryptophan (7h): Yield 91%; Mp 164-166°C; Off white solid; FT IR (ATR, υ_{max}, cm^{-1}): 3409 (O-H), 3056 (Ar-H), 2933 and 2858 (C-H), 1720 (C=O of acid), 1641 (C=O of amide), 1614 (C=N), 1527 (C=C), 1296 (C-O), 1230 (C-F); ^{1}H NMR (400 MHz, DMSO-d_6, δ ppm): 10.79 (s, 1H, indole-NH), 8.52 (d, 1H, amide-NH, J = 7.6 Hz), 8.2 (d, 1H, Ar-H, J = 1.2 Hz), 7.90 (d, 1H, Ar-H, J = 8.8 Hz), 7.71-7.76 (m, 3H, Ar-H), 7.62 (d, 1H, Ar-H, J = 8.0 Hz), 7.44 (m, 2H, Ar-H, J = 8.8 Hz), 7.32 (d, 1H, Ar-H, J = 8.0 Hz), 7.22 (d, 1H, Ar-H, J = 2.0 Hz), 7.03-7.07 (m, 1H, Ar-H); 6.95-6.99 (m, 1H, Ar-H); 4.63-4.68 (m, 1H, chiral C-H), 4.19-4.25 (m, 1H, -NC-H), 3.33-3.38 (dd, 1H, indole CH_2, J = 4.2 and 14.6 Hz), 3.23-3.29 (dd, 1H, indole CH_2, J = 9.2 and 14.4 Hz), 2.22-2.31 (m, 2H, cyclohexyl),

1.82-1.92 (m, 4H, cyclohexyl), 1.62-1.65 (m, 1H, cyclohexyl), 1.26-1.40 (m, 3H, cyclohexyl); ^{13}C NMR (100 MHz, DMSO-d_6, δ ppm): 173.8, 166.3, 164.2, 161.7, 153.7, 142.6, 136.0, 135.6, 131.8, 131.7, 128.0, 127.3, 126.9, 123.5, 121.7, 120.8, 118.7, 118.3, 118.2, 115.9, 115.7, 112.6, 111.3, 110.7, 56.8, 54.1, 30.5, 26.8, 25.4, 24.3; ESI-MS (*m/z*): 524.22 $[M+H]^+$; Anal. calcd. for $C_{31}H_{29}N_4FO_3$: C, 70.98; H, 5.57; N, 10.68. Found: C, 70.95; H, 5.58; N, 10.66.

(S)-(2-(2-Chloro-6-fluorophenyl)-1-cyclohexyl-1H-benzo[d]imidazole-5-carbonyl)alanine (7i): Yield 70%; Mp 248-250°C; Off white solid; IR (ATR, υ_{max}, cm^{-1}): 3372 (O-H), 3078 (Ar-H), 2948 and 2862 (C-H), 1721 (C=O of acid), 1642 (C=O of amide), 1620 (C=N), 1576 (C=C), 1296 (C-O), 1247 (C-F); ^{1}H NMR (400 MHz, DMSO-d_6, δ ppm): 8.61 (d, 1H, amide N-H, J = 8.0 Hz), 8.34 (s, 1H, Ar-H), 7.97 (d, 1H, Ar-H, J = 8.4 Hz), 7.87 (d, 1H, Ar-H, J = 8.8 Hz), 7.71-7.77 (m, 1H, Ar-H), 7.62 (m, 1H, Ar-H), 7.49-7.54 (m, 1H, Ar-H), 4.63-4.68 (m, 1H, chiral CH), 4.19-4.25 (m, 1H, N-CH), 2.22-2.31 (m, 2H, cyclohexyl), 1.82-1.92 (m, 4H, cyclohexyl), 1.62-1.65 (m, 1H, cyclohexyl), 1.42-1.44 (d, 3H, CH_3, J = 7.2 Hz), 1.26-1.40 (m, 3H, cyclohexyl); ^{13}C NMR (100 MHz, DMSO-d_6, δ ppm): 174.4, 166.4, 162.8, 160.5, 146.8, 143.7, 136.5, 132.3, 132.2, 125.5, 124.5, 124.0, 122.9, 119.4, 119.2, 114.5, 114.3, 111.9, 56.7, 48.2, 30.5, 25.5, 24.4, 16.9; ESI-MS (*m/z*): 444.4 $[M+H]^+$, 446.4 $[M+2+H]^+$; Anal. calcd. for $C_{23}H_{23}N_3ClFO_3$: C, 62.23; H, 5.22; N, 9.47. Found: C, 62.25; H, 5.21; N, 9.45.

(S)-(2-(2-Chloro-6-fluorophenyl)-1-cyclohexyl-1H-benzo[d]imidazole-5-carbonyl)valine (7j): Yield 81%; Mp 88-90°C; Off white solid; IR (ATR, υ_{max}, cm^{-1}): 3362 (O-H), 3073 (Ar-H), 2947 and 2861 (C-H), 1724 (C=O of acid), 1644 (C=O of amide), 1621 (C=N), 1574 (C=C), 1297 (C-O), 1246 (C-F); ^{1}H NMR (400 MHz, DMSO-d_6, δ ppm): 8.61 (d, 1H, amide N-H, J = 8.0 Hz), 8.34 (s, 1H, Ar-H), 7.97 (d, 1H, Ar-H, J = 8.4 Hz), 7.87 (d, 1H, Ar-H, J = 8.8 Hz), 7.71-7.77 (m, 1H, Ar-H), 7.62 (m, 1H, Ar-H), 7.49-7.54 (m, 1H, Ar-H), 4.29-4.32 (m, 1H, chiral CH), 4.26-4.28 (m, 1H, N-CH), 2.25-2.33 (m, 2H, cyclohexyl), 2.20-2.25 (m, 1H, C-H of isopropyl), 1.84-1.90 (m, 4H, cyclohexyl), 1.63-1.66 (m, 1H, cyclohexyl), 1.24-1.41 (m, 3H, cyclohexyl), 0.97-1.01 (m, 6H, diastereotopic CH_3); ^{13}C NMR (100 MHz, DMSO-d_6, δ ppm): 174.4, 166.4, 162.9, 160.5, 146.8, 143.7, 136.5, 132.3, 132.2, 125.5, 124.5, 122.9, 119.4, 119.2, 114.4, 114.2, 111.9, 58.7, 56.6, 30.5, 29.6, 25.5, 24.4, 19.4, 18.9; ESI-MS (*m/z*): 472.4 $[M+H]^+$, 474.4 $[M+2+H]^+$; Anal. calcd. for $C_{25}H_{27}N_3ClFO_3$: C, 63.62; H, 5.77; N, 8.90. Found: C, 63.60; H, 5.74; N, 8.91.

(S)-(2-(2-Chloro-6-fluorophenyl)-1-cyclohexyl-1H-benzo[d]imidazole-5-carbonyl)leucine (7k): Yield 98%; Mp 124-126°C; Off white solid; IR (ATR, υ_{max}, cm^{-1}): 3355 (O-H), 3080 (Ar-H), 2948 and 2864 (C-H), 1722 (C=O of acid), 1643 (C=O of amide), 1620 (C=N), 1571 (C=C), 1299 (C-O), 1249 (C-F); ^{1}H NMR (400 MHz, DMSO-d_6, δ ppm): 12.51 (s, 1H, CO_2H), 8.61 (d, 1H, amide N-H, J = 8.0 Hz), 8.34 (s, 1H, Ar-H), 7.97 (d, 1H, Ar-H, J = 8.4 Hz), 7.87 (d, 1H, Ar-H, J = 8.8 Hz), 7.71-7.77 (m, 1H, Ar-H), 7.62 (m, 1H, Ar-H), 7.49-7.54 (m, 1H, Ar-H), 4.47-4.51 (m, 1H, chiral C-H), 3.84-3.90 (m, 1H, N-CH), 2.12-2.21 (m, 2H, cyclohexyl), 1.60-1.84 (m, 8H, cyclohexyl, isobutyl CH and diastereotopic CH_2), 1.24-1.29 (m, 3H, cyclohexyl), 0.94 (d, 3H, diastereotopic CH_3, J = 6.4 Hz), 0.90 (d, 3H, diastereotopic CH_3, J = 6.4 Hz); ^{13}C NMR (100 MHz, DMSO-d_6, δ ppm): 174.4, 166.4, 162.8, 160.5, 146.8, 143.7, 136.5, 132.3, 132.2, 125.5, 124.5, 124.0, 122.9, 119.4, 119.2, 114.5, 114.3, 111.9, 56.6, 50.9, 30.5, 25.5, 24.6, 24.3, 23.1, 21.6; ESI-MS (*m/z*): 485.4 $[M+H]^+$, 487.4 $[M+2+H]^+$; Anal. calcd. for $C_{26}H_{29}N_3ClFO_3$: C, 64.26; H, 6.01; N, 8.65. Found: C, 64.25; H, 6.03; N, 8.66.

(S)-(2-(2-Chloro-6-fluorophenyl)-1-cyclohexyl-1H-benzo[d]imidazole-5-carbonyl)tryptophan (7l): Yield 97%; Mp 182-184°C; Off white solid; FT IR (ATR, υ_{max}, cm^{-1}): 3409 (O-H), 3056 (Ar-H), 2937 and 2858 (C-H), 1724 (C=O of acid), 1641 (C=O of amide), 1620 (C=N), 1573 (C=C), 1299 (C-O), 1251 (C-F); ^{1}H NMR (400 MHz, DMSO-d_6, δ ppm): 10.80 (s, 1H, indole-NH), 8.67 (d, 1H, amide N-H, J = 7.6 Hz), 8.27 (s, 1H, Ar-H), 7.95 (d, 1H, Ar-H, J = 8.4 Hz), 7.71-7.80 (m, 2H, Ar-H), 7.60-7.63 (m, 2H, Ar-H), 7.49-7.53 (m, 1H, Ar-H), 7.32 (d, 1H, Ar-H, J = 8.0 Hz), 7.23 (s, 1H, Ar-H), 7.04-7.08 (m, 1H, Ar-H), 6.98-7.01 (m, 1H, Ar-H), 4.67-4.72 (m, 1H, chiral C-H), 3.83-3.89 (m, 1H, N-CH), 3.22-3.28 (m, 2H, indolyl CH_2), 2.07-2.18 (m, 2H, cyclohexyl), 1.79-1.90 (m, 4H, cyclohexyl), 1.59-1.61 (m, 1H, cyclohexyl), 1.17-1.28 (m, 3H, cyclohexyl); ^{13}C NMR (100 MHz, DMSO-d_6, δ ppm): 173.6, 166.6, 161.9, 159.5, 145.8, 142.8, 136.2, 135.1, 134.8, 133.6, 128.1, 127.2, 125.9, 123.6, 122.5, 120.9, 119.4, 119.2, 118.4, 118.1, 114.9, 114.7, 112.3, 111.5, 110.5, 57.2, 53.9, 30.8, 26.6, 25.3, 24.3; ESI-MS (*m/z*): 559.3 $[M+H]^+$, 561.3 $[M+2+H]^+$; Anal. calcd. for $C_{31}H_{28}N_4ClFO_3$: C, 66.60; H, 5.05; N, 10.02. Found: C, 66.57; H, 5.08; N, 10.01.

General procedure for the synthesis of 3-aryl-1*H*-pyrazole-4-carboxaldehydes (10a-c)

3-Aryl-1*H*-pyrazole-4-carboxaldehydes **(10a-c)** were prepared according to the general procedure described in the literature[11] by means of Vilsmeier-Haack reaction on 2-(1-

arylethylidene)hydrazinecarboxamides **(9a-c)** which in-turn were prepared by the reaction of substituted acetophenones **(8a-c)** with semicarbazide hydrochloride in acetic acid-sodium acetate buffer. In a typical experiment, to an ice-cold solution of (1-arylethylidene) hydrazinecarboxamides **(9a-c)** (10 mmol) in DMF (20 mL), $POCl_3$ (50 mmol) was added dropwise with stirring at 0 °C. After complete addition, the reaction mass was stirred at room temperature for about 30 min and then at 60-65 °C for 8 h. The reaction mixture was allowed to cool to room temperature and then quenched with crushed ice, followed by neutralization with 25% sodium hydroxide solution. The solid obtained was filtered, washed with water and dried. The crude product was used as such for the next step.

General procedure for the synthesis of 2-(4-oxo-2-thioxothiazolidin-3-yl)amino acids (12a-d)

2-(4-Oxo-2-thioxothiazolidin-3-yl)amino acids **(12a-d)** were prepared according to the reported procedure.[21] Appropriate amino acid **(11a-d,** 10 mmol) was dissolved in a solution of potassium hydroxide (10 mmol) in water (10 mL). Carbon disulfide (10 mmol) was added dropwise to the above clear solution and stirred at room temperature for 6-12 h. An aqueous solution of potassium chloroacetate (10 mmol) was then added and continued stirring for further 30 min. The reaction mixture was acidified with 2N HCl to pH 3.0 and stirred at 90 °C for 1-3 h. The reaction mixture was poured onto crushed ice and solid obtained was filtered, washed with water, dried and used as such for the next step. Whenever a gummy solid was obtained, it was extracted to ethyl acetate, concentrated *in vacuo* and triturated with hexane to get orange solid.

General procedure for the synthesis of pyrazole conjugated rhodanine carboxylic acids (13a-l)

β-Alanine (0.02 mol, 2.0 equiv.) was added to a clear solution of pyrazole aldehyde (**10a-c**, 0.01 mol, 1.0 equiv.) and rhodanine amino acid (**12a-d**, 0.01 mol, 1.0 equiv.) in acetic acid (10 mL). Then the reaction mixture was heated to reflux for 16-18 h. After completion of the reaction (monitored by TLC hexane: ethyl acetate (2:1, v/v)), the reaction mass was allowed to cool to room temperature and poured onto crushed ice to get yellow to orange colored solid. The solid separated was filtered, washed with water, dried and subjected to column purification (10 to 50 % ethyl acetate in hexane) to obtain pure product.

(S)-2-(5-((3-(4-Methoxyphenyl)-1H-pyrazol-4-yl)methylene)-4-oxo-2-thioxothiazolidin-3-yl)acetic acid (13a): Yield 60%; Mp 164-166 °C; Red solid; FT IR (ATR, υ_{max}, cm^{-1}): 3400 (O-H), 3001 (Ar-H), 2933 and 2858 (C-H), 1705 (C=O), 1610 (C=N), 1529 (C=C), 1228 (C=S), 1106 (C-O); ^{1}H NMR (400 MHz, DMSO-d_6, δ ppm): 8.05 (s, 1H, pyrazole-5H), 7.53 (s, 1H, =C-H), 7.49 (d, 2H, Ar-H, J = 8.4 Hz), 7.12 (d, 2H, Ar-H, J = 8.8 Hz), 3.57 (s, 2H, CH_2); ^{13}C NMR (100 MHz, DMSO-d_6, δ ppm): 192.1, 169.6, 166.0, 160.1, 130.1, 125.4, 117.4, 114.6, 112.8, 55.3, 43.1; ESI-MS (*m/z*): 374.2 $[M-H]^-$; Anal. calcd. for $C_{16}H_{13}N_3O_4S_2$: C, 51.19; H, 3.49; N, 11.19. Found: C, 51.21; H, 3.46; N, 11.14.

(S)-2-(5-((3-(4-Methoxyphenyl)-1H-pyrazol-4-yl)methylene)-4-oxo-2-thioxothiazolidin-3-yl)propanoic acid (13b): Yield 65%; Mp 150-152 °C; Red solid; FT IR (ATR, υ_{max}, cm^{-1}): 3496 (O-H), 3172 (Ar-H), 2903 and 2856 (C-H), 1709 (C=O), 1608 (C=N), 1516 (C=C), 1247 (C=S), 1111 (C-O); ^{1}H NMR (400 MHz, DMSO-d_6, δ ppm): 8.05 (s, 1H, pyrazole-5H), 7.53 (s, 1H, =C-H), 7.49 (d, 2H, Ar-H, J = 8.4 Hz), 7.12 (d, 2H, Ar-H, J = 8.8 Hz), 5.55-5.61 (q, 1H, J = 7.2 Hz), 3.82 (s, 3H, OCH_3), 1.51 (d, 3H, CH_3, J = 6.8 Hz); ^{13}C NMR (100 MHz, DMSO-d_6, δ ppm): 192.1, 169.6, 166.0, 160.1, 130.1, 125.4, 117.4, 114.6, 112.8, 55.3, 52.8, 13.4; ESI-MS (*m/z*): 388.2 $[M-H]^-$; Anal. calcd. for $C_{17}H_{15}N_3O_4S_2$: C, 52.43; H, 3.88; N, 10.79. Found: C, 52.41; H, 3.85; N, 10.81.

(S)-2-(5-((3-(4-Methoxyphenyl)-1H-pyrazol-4-yl)methylene)-4-oxo-2-thioxothiazolidin-3-yl)-3-phenylpropanoic acid (13c): Yield 48%; Mp 122-124 °C; Red solid; FT IR (ATR, υ_{max}, cm^{-1}): 3279 (O-H), 3001 (Ar-H), 2933 and 2858 (C-H), 1702 (C=O), 1610 (C=N), 1529 (C=C), 1250

(C=S), 1172 (C-O); ^{1}H NMR (400 MHz, DMSO-d_6, δ ppm): 7.86 (s, 1H, pyrazole-5H), 7.32-7.35 (m, 3H, Ar-H), 6.92-7.12 (m, 7H, Ar-H, =C-H, Ph), 5.67 (overlapped multiplet, 1H, chiral CH), 3.68 (s, 3H, OCH_3), 3.13-3.16 (m, 2H, CH_2); ^{13}C NMR (100 MHz, DMSO-d_6, δ ppm): 192.1, 169.6, 166.0, 160.1, 136.5, 130.1, 128.9, 128.2, 126.7, 125.4, 117.4, 114.6, 112.8, 58.1, 55.3, 33.1; ESI-MS (*m/z*): 464.2 $[M-H]^-$; Anal. calcd. for $C_{23}H_{19}N_3O_4S_2$: C, 59.34; H, 4.11; N, 9.03. Found: C, 59.31; H, 4.10; N, 9.05.

(S)-3-(1H-Indol-3-yl)-2-(5-((3-(4-methoxyphenyl)-1H-pyrazol-4-yl)methylene)-4-oxo-2-thioxothiazolidin-3-yl)propanoic acid (13d): Yield 85%; Mp 160-162 °C; Red solid; FT IR (ATR, υ_{max}, cm^{-1}): 3274 (O-H), 3001 (Ar-H), 2929 and 2853 (C-H), 1705 (C=O), 1608 (C=N), 1513 (C=C), 1253 (C=S), 1177 (C-O); ^{1}H NMR (400 MHz, DMSO-d_6, δ ppm): 10.77 (s, 1H, indole NH), 7.98 (s, 1H, pyrazole-5H), 7.45-7.49 (m, 4H, Ar-H, =C-H), 7.27-7.29 (m, 1H, Ar-H), 7.12-7.15 (d, 2H, Ar-H, J = 8.4 Hz), 6.99-7.05 (m, 2H, Ar-H), 6.89-6.93 (m, 1H, Ar-H), 5.86 (overlapped multiplet, 1H, chiral CH), 3.83 (s, 3H, OCH_3), 3.56-3.61 (dd, 2H, CH_2, J = 14.8 Hz and 5.2 Hz); ^{13}C NMR (100 MHz, DMSO-d_6, δ ppm): 192.1, 169.1, 166.3, 160.1, 135.9, 130.1, 127.1, 125.2, 123.7, 120.9, 118.4, 117.8, 114.6, 112.7, 111.3, 108.9, 58.0, 55.3, 23.0; ESI-MS (*m/z*): 503.2 $[M-H]^-$; Anal. calcd. for $C_{25}H_{20}N_4O_4S_2$: C, 59.51; H, 4.00; N, 11.10. Found: C, 59.49; H, 4.10; N, 11.06.

(S)-2-(5-((3-(4-Nitrophenyl)-1H-pyrazol-4-yl)methylene)-4-oxo-2-thioxothiazolidin-3-yl)acetic acid (13e): Yield 72%; Mp 136-138 °C; Yellow solid; FT IR (ATR, υ_{max}, cm^{-1}): 3332 (O-H), 3116 (Ar-H), 2967 and 2856 (C-H), 1703 (C=O), 1601 (C=N), 1548 (C=C), 1332 (N=O), 1241 (C=S), 1127 (C-O); ^{1}H NMR (400 MHz, DMSO-d_6, δ ppm): 8.40 (d, 2H, Ar-H, J = 8.0 Hz), 8.30 (s, 1H, pyrazole-5H), 7.87 (d, 2H, Ar-H, J = 8.4 Hz), 7.56 (s, 1H, =C-H), 3.56 (s, 2H, CH_2); ^{13}C NMR (100 MHz, DMSO-d_6, δ ppm): 192.1, 169.6, 165.9, 147.4, 129.8, 124.3, 124.1, 119.3, 113.6, 43.1; ESI-MS (*m/z*): 479.2 $[M-H]^-$; Anal. calcd. for $C_{15}H_{10}N_4O_5S_2$: C, 46.15; H, 2.58; N, 14.35. Found: C, 46.12; H, 2.55; N, 14.29.

(S)-2-(5-((3-(4-Nitrophenyl)-1H-pyrazol-4-yl)methylene)-4-oxo-2-thioxothiazolidin-3-yl)propanoic acid (13f): Yield 68%; Mp 240-242 °C; Yellow solid; FT IR (ATR, υ_{max}, cm^{-1}): 3223 (O-H), 3116 (Ar-H), 2967 and 2862 (C-H), 1702 (C=O), 1601 (C=N), 1548 (C=C), 1336 (N=O), 1247 (C=S), 1127 (C-O); ^{1}H NMR (400 MHz, DMSO-d_6, δ ppm): 8.39 (d, 2H, Ar-H, J = 8.4 Hz),

8.30 (s, 1H, pyrazole-5H), 7.87 (d, 2H, Ar-H, *J* = 8.8 Hz), 7.58 (s, 1H, =C-H), 5.56-5.62 (q, 1H, chiral CH, *J* = 7.2 Hz), 1.52 (d, 3H, CH_3, *J* = 6.8 Hz); ^{13}C NMR (100 MHz, DMSO-d_6, δ ppm): 192.1, 169.5, 165.9, 147.4, 129.7, 124.3, 124.1, 119.3, 113.6, 52.8, 13.3; ESI-MS (*m/z*): 403.2 [M-H]$^-$; Anal. calcd. for $C_{16}H_{12}N_4O_5S_2$: C, 47.52; H, 2.99; N, 13.85. Found: C, 47.55; H, 2.96; N, 13.82.

(S)-2-(5-((3-(4-Nitrophenyl)-1H-pyrazol-4-yl)methylene)-4-oxo-2-thioxothiazolidin-3-yl)-3-phenylpropanoic acid (13g): Yield 67%; Mp 90-92 °C; Yellow solid; FT IR (ATR, υ_{max}, cm^{-1}): 3256 (O-H), 3025 (Ar-H), 2921 and 2851 (C-H), 1713 (C=O), 1601 (C=N), 1337 (N=O), 1230 (C=S), 1107 (C-O); ^{1}H NMR (400 MHz, DMSO-d_6, δ ppm): 8.40 (d, 2H, Ar-H, J = 8.0 Hz), 8.30 (s, 1H, pyrazole-5H), 7.87 (d, 2H, Ar-H, *J* = 8.4 Hz), 7.56 (s, 1H, =C-H), 7.13-7.2 (m, 5H, Ar-H), 5.86 (overlapped multiplet, 1H, chiral CH), 2.09 (s, 2H, CH2); ^{13}C NMR (100 MHz, DMSO-d_6, δ ppm): 192.1, 168.7, 166.1, 147.4, 136.5, 129.7, 128.9, 128.2, 126.7, 124.4, 124.1, 118.6, 113.5, 58.1, 33.1; ESI-MS (*m/z*): 479.2 [M-H]$^-$; Anal. calcd. for $C_{22}H_{16}N_4O_5S_2$: C, 54.99; H, 3.36; N, 11.66. Found: C, 54.96; H, 3.38; N, 11.63.

(S)-3-(1H-indol-3-yl)-2-(5-((3-(4-nitrophenyl)-1H-pyrazol-4-yl)methylene)-4-oxo-2-thioxothiazolidin-3-yl)propanoic acid (13h): Yield 83%; Mp 152-154 °C; Yellow solid; FT IR (ATR, υ_{max}, cm^{-1}): 3271 (O-H), 3023 (Ar-H), 2928 and 2852 (C-H), 1713 (C=O), 1603 (C=N), 1334 (N=O), 1231 (C=S), 1108 (C-O); ^{1}H NMR (400 MHz, DMSO-d_6, δ ppm): 10.84 (s, 1H, indole-NH), 8.47 (d, 2H, Ar-H, *J* = 8.3 Hz), 8.38 (s, 1H, pyrazole-5H), 7.92 (d, 2H, Ar-H, *J* = 8.5 Hz), 7.59 (s, 1H, =C-H), 7.53 (d, 1H, Ar-H, *J* = 7.6 Hz), 7.33 (d, 1H, Ar-H, *J* = 8.0 Hz), 7.11 (s, 1H, Ar-H), 7.05-7.09 (m, 1H, Ar-H), 6.95-6.99 (m, 1H, Ar-H), 5.91 (overlapped multiplet, 1H, chiral CH), 3.62-3.67 (dd, 2H, CH_2, *J* = 15.2 Hz and 5.2 Hz); ^{13}C NMR (100 MHz, DMSO-d_6, δ ppm): 192.1, 169.4, 166.1, 147.6, 135.9, 129.7, 127.1, 124.3, 124.1, 123.7, 120.9, 119.3, 118.4, 117.8, 113.6, 111.3, 108.9, 55.3, 23.0; ESI-MS (*m/z*): 518.2 [M-H]$^-$; Anal. calcd. for $C_{24}H_{17}N_5O_5S_2$: C, 55.48; H, 3.30; N, 13.48. Found: C, 55.44; H, 3.28; N, 13.45.

(S)-2-(5-((3-(3,5-Difluorophenyl)-1H-pyrazol-4-yl)methylene)-4-oxo-2-thioxothiazolidin-3-yl)acetic acid (13i): Yield 83%; Mp 108-110 °C; Yellow solid; FT IR (ATR, υ_{max}, cm^{-1}): 3325 (O-H), 3001 (Ar-H), 2929 and 2848 (C-H), 1703 (C=O), 1605 (C=N), 1512 (C=C), 1253 (C=S), 1122 (C-F), 1060 (C-O); ^{1}H NMR (400 MHz, DMSO-d_6, δ ppm): 8.16 (s, 1H, pyrazole-5H), 7.51 (s,

1H, =C-H), 7.29-7.38 (m, 3H, Ar-H), 3.57 (s, 2H, CH_2); ^{13}C NMR (100 MHz, DMSO-d_6, δ ppm): 192.1, 169.2, 166.2, 163.8, 163.7, 161.4, 161.2, 124.4, 119.0, 113.3, 111.9, 111.8, 111.7. 111.6, 104.4, 43.1; ESI-MS (*m/z*): 374.2 $[M-H]^-$; Anal. calcd. for $C_{15}H_9N_3F_2O_3S_2$: C, 47.24; H, 2.38; N, 11.02. Found: C, 47.27; H, 2.35; N, 11.04.

(S)-2-(5-((3-(3,5-Difluorophenyl)-1H-pyrazol-4-yl)methylene)-4-oxo-2-thioxothiazolidin-3-yl)propanoic acid (13j): Yield 57%; Mp 110-112 °C; Yellow solid; FT IR (ATR, υ_{max}, cm^{-1}): 3246 (O-H), 3087 (Ar-H), 2922 and 2858 (C-H), 1712 (C=O), 1604 (C=N), 1534 (C=C), 1243 (C=S), 1120 (C-F), 1056 (C-O); ^{1}H NMR (400 MHz, DMSO-d_6, δ ppm): 8.21 (s, 1H, pyrazole-5H), 7.55 (s, 1H, =C-H), 7.29-7.38 (m, 3H, Ar-H), 5.55-5.61 (q, 1H, chiral CH, J = 7.2 Hz), 1.52 (d, 3H, CH_3, J = 7.2 Hz); ^{13}C NMR (100 MHz, DMSO-d_6, δ ppm): 192.1, 169.5, 165.9, 163.8, 163.7, 161.4, 161.2, 124.4, 118.9, 113.3, 111.9, 111.8, 111.7, 111.6, 104.3, 52.8, 13.3; ESI-MS (*m/z*): 394.2 $[M-H]^-$; Anal. calcd. for $C_{16}H_{11}N_3F_2O_3S_2$: C, 48.60; H, 2.80; N, 10.63. Found: C, 48.57; H, 2.81; N, 10.66.

(S)-2-(5-((3-(3,5-Difluorophenyl)-1H-pyrazol-4-yl)methylene)-4-oxo-2-thioxothiazolidin-3-yl)-3-phenylpropanoic acid (13k): Yield 61%; Mp 114-116 °C; Yellow solid; FT IR (ATR, υ_{max}, cm^{-1}): 3253 (O-H), 3025 (Ar-H), 2924 and 2858 (C-H), 1716 (C=O), 1604 (C=N), 1535 (C=C), 1230 (C=S), 1122 (C-F); ^{1}H NMR (400 MHz, DMSO-d_6, δ ppm): 8.29 (s, 1H, pyrazole-5H), 7.54 (s, 1H, =C-H), 7.32-7.41 (m, 3H, Ar-H), 7.14-7.22 (m, 5H, Ar-H), 5.85 (overlapped multiplet, 1H, chiral CH), 3.29-3.33 (m, 2H, CH_2); ^{13}C NMR (100 MHz, DMSO-d_6, δ ppm): 192.2, 168.7, 166.2, 163.8, 163.7, 161.4, 161.2, 136.5, 128.9, 128.2, 126.6, 124.6, 118.3, 113.2, 111.9, 111.7, 104.3, 58.2, 33.1; ESI-MS (*m/z*): 470.2 $[M-H]^-$; Anal. calcd. for $C_{22}H_{15}N_3F_2O_3S_2$: C, 56.04; H, 3.21; N, 8.91. Found: C, 56.01; H, 3.24; N, 8.89.

(S)-2-(5-((3-(3,5-Difluorophenyl)-1H-pyrazol-4-yl)methylene)-4-oxo-2-thioxothiazolidin-3-yl)-3-(1H-indol-3-yl)propanoic acid (13l): Yield 83%; Mp 120-122 °C; Yellow solid; FT IR (ATR, υ_{max}, cm^{-1}): 3411 (O-H), 3081 (Ar-H), 2924 and 2858 (C-H), 1709 (C=O), 1604 (C=N), 1534 (C=C), 1223 (C=S), 1121 (C-F); ^{1}H NMR (400 MHz, DMSO-d_6, δ ppm): 10.77 (s, 1H, indole-NH), 8.16 (s, 1H, pyrazole-5H), 7.51 (s, 1H, =C-H),7.45-7.47 (m, 1H, Ar-H), 7.36-7.45 (m, 1H, Ar-H), 7.26-7.30 (m, 3H, Ar-H), 6.99-7.05 (m, 2H, Ar-H), 6.89-6.92 (m, 1H, Ar-H), 5.86 (s, 1H, chiral C-H), 3.56-3.61 (dd, 2H, CH_2, J = 14.8 Hz and 4.8 Hz); ^{13}C NMR (100 MHz, DMSO-d_6, δ

ppm): 192.1, 169.0, 166.2, 163.8, 163.7, 161.4, 161.2, 135.9, 127.0, 124.2, 123.7, 120.9, 118.6, 118.4, 117.8, 113.2, 111.9, 111.8, 111.7, 111.6, 111.3, 108.9, 104.4, 58.1, 23.0; ESI-MS (*m/z*): 509.2 $[M-H]^-$; Anal. calcd. for $C_{24}H_{16}N_4F_2O_3S_2$: C, 56.46; H, 3.16; N, 10.97. Found: C, 56.42; H, 3.18; N, 10.94.

Biological evaluation:

Evaluation of Sirt1/2/3 inhibition activity. Test and standard compounds at a concentration of 10 µM were incubated with 5 IU of Recombinant Human SIRT1/2/3 protein and SIRT1 substrate (Flour-delys-SIRT1)/Sirt2 substrate (Flour-delys-SIRT2)/Sirt3 substrate (Flour-delys-SIRT2) at a concentration of 25 µM in presence of 200 µM of NAD+ for 10 to 15 min. After taking the initial fluorescence value at 360/460 nm excitation/emission wavelength, the sample mixture was incubated at 37 °C for 30 minutes. After completion of the incubation period, developing solution was added to the reaction mixture and florescence was observed at 360/460 nm excitation/emission wavelength. Percentage inhibition of Sirt 1/2/3 was calculated.

Determination of IC_{50} value of Sirt1 activity. Different concentrations (ranges from 50 nm to 1000 nm) of test and standard compounds were incubated with 5 IU of Recombinant Human Sirt1 protein and with substrate (Flour-delys-Sirt1) at a concentration of 25 µM in the presence of 200 µM of NAD+ as recommended by the manufacturer kit (Enzo life sciences cat. No. BML-AK55). Initial fluorescence was taken at 360/460 nm Excitation/Emission wavelength before incubating the sample at 37 °C for 30 minutes. Developing solution was added to the reaction mixture and the florescence was observed at 360/460 nm excitation/emission wavelength. Percentage inhibition of Sirt1 was calculated, the concentration-response curve was plotted and IC50 was determined.

Evaluation of SIRT1/2 and 3 inhibition activity in HepG2 cells. HepG2 cells were obtained from ATCC and maintained in DMEM media with 10 % FBS and 1 µg/mL pen strip antibiotic at 37 °C and 5% CO_2 and 95 % O_2. To evaluate the Sirt1 and 2/3 activity, cells were treated with test and standard compounds at a concentration of 10 µM for 6 h. After 6 h, the cells were washed with PBS, lysed with lysis buffer and measured the Sirt1 and 2/3 activity using the cell lysate as discussed before.

Western blotting. HepG2, a human liver cancer cells (ATCC) were grown under standard conditions. Cells were treated with the test compounds at a concentration of 25 µM for 48 h. Cells were lysed and protein samples were prepared with RIPA buffer. Western blots were carried out

to determine the levels of acetylated p53 and Sirt1 in treated cells. Primary antibody for acetylated-p53 (Abcam cat.no ab61241) and Sirt1 (Cell signaling cat.no.#9475), and secondary antibody were used at dilutions recommended by the manufacturer.

Cell Viability Assays. Cell lines (HepG2, Caco2, and MCF7) were obtained from ATCC and were grown under standard conditions. To perform cell viability assays, cells were seeded into 96-well plates and treated with test compounds in DMSO (final DMSO concentration 0.25%). Cells were incubated with test compounds at different concentrations (1, 10, 100, 200, 300, and 400 µM , or DMSO control) for 24 h, then cells were incubated with 10 µL of 2 mg/mL MTT (Merck millipore, cat no. 475989) solution in PBS for about 2 to 3 h, then MTT solution was aspirated from the plate and 50 µL of DMSO was added to each well and plates were kept on rocking shaker for 30 min, absorbance was taken at 570 nm, % viability was determined. Assays were carried out in triplicate. Reported values are averages of two independent experiments.

***In-Silico* Computational Methods:**

All calculations were performed, on a Linux Centos7.0 based Workstation (RAM 132GB, CPU-core 8, GPU-card 1 GTX1080) and Linux Centos 6.9 based Server (RAM 64GB, CPU(S) 64, GPU(S) 2 Tesla-P100), by using the Maestro release 2017-2 graphical user interface (GUI) of the Schrodinger software suite[54], VMD 1.9.3[55], ChemDraw Professional 15.1.[56] and Desmond-3.7[57].

Ligand Preparation. All Ligands were drawn by ChemDraw Professional 15.1, and then, LigPrep (**LigPrep, Maestro** 11.2.014, Schrödinger LLC) with OPLS3[58] force field, was used to build ligands, generate stereoisomers and tautomers. Further, ligands were desalted and protonated at pH 7.0 ± 2.0 through the tool Epik (Shelley et al., 2007) module. For other parameters, the default values were assigned. Qikprop, Lipinsnki's rule of five and reactive functional group screening were performed to check the drug likiness of ligands.[59]

Cheminformatic Analysis: Molecular weight and cLogP for all compounds were calculated by by ChemDraw.

Selection of structures and molecular modeling. Presently, two X-ray crystal structures available for Sirt1-inhibitor complex in the Protein Data Bank (PDB), and their PDB id's are 4I5I and 4ZZI. Both structures were imported and prepared in maestro, further enrichment calculation was performed to select the best structure for the docking studies. A total of 1000 decoys molecule and, three actives (reported inhibitor) Ex527, Ex527-anlogue (PDB id 4I5I) and 4TO (PDB id

4ZZI) were used to calculate enrichment and receiver operating characteristics (ROC) plot. Finally, molecular modeling was performed to get the final protein-ligand complex for further study.[60]

Protein Preparation and Grid Generation. Structures were prepared through the Protein Preparation Wizard Workflow, Maestro module of Schrödinger software. Protein Preparation Wizard Workflow performed the basic preparation tasks, like proper assignment of bonds, addition of hydrogen, creation of zero-order bong to metals, disulfide bonds creation, and deletion of water molecules beyond 5 Å from the het group, in step by step way. After protein preparation, water sampling and basic restrain minimization that allows only hydrogen atoms to be freely minimized was performed by using force field OPLS3.[61]

Subsequently, with the help of Glide (**Glide, Maestro** 11.2.014, Schrödinger LLC), receptor grids of these complexes were generated. A virtual grid box of volume 20 × 20 × 20 Å region in space centred at the original ligand of the complex structures was consider generating receptor grid. For the other parameters, the default values were assigned.[62]

Selection of Docking Model and Docking. Docking was performed with Glide in extra precision (XP) mode at pre-defined grid with flexible ligand sampling and epic state penalties and other parameters were set to default.

Pose correction Binding Pose Metadynamics. To find the correct binding pose of ligands at the binding pocket, we have run a series of metadynamics MD simulations for "2ns" on each set of docked protein-ligand complex. Binding pose metadynamics, was performed through Desmond metadynamics MD simulation, it evaluates the comparative stability of binding pose. Total 10 no. of trial per pose was selected to perform the study.

MMGBSA Binding Energy calculation. Binding free energy of protein-ligand docked complex (ΔG_{bind}) was calculated by MM-GBSA protocol through Prime (**Prime, Maestro** 11.2.014, Schrödinger LLC). MM-GBSA calculation was performed for each protein ligand complex and control, by using force field, OPLS3 and salvation model, variable-dielectric generalized Born (VSGB) model[63]. We used this $\mathbf{\Delta G_{bind}}$ to rank protein-ligand docked complex and ligand showing the highest negative value selected as best ligands for further biological study.

The per-residue energy decomposition of MD system was calculated through MM(GB/PB)SA protocol implemented in Amber.[64] Total 200 snapshots extracted from equilibrated trajectory of

each system and binding energy was calculated through MMGBSA.py script implemented in amber.

$\Delta G_{bind,}$ is the total sum of difference in minimized energy (ΔE_{MM}), difference in solvation energy (ΔG_{solv}), and difference in surface area energy.

$$\Delta G_{bind} = \Delta E_{MM} + \Delta G_{solv} + \Delta G_{SA}$$

$$\Delta E_{MM} = E_{min\ (complex)} - (E_{min\ (protein)} + E_{min\ (ligand)})$$

$$\Delta G_{solv} = G_{solv\ (complex)} - (G_{solv\ (protein)} + G_{solv\ (ligand)})$$

$$\Delta G_{SA} = G_{SA\ (complex)} - (G_{SA\ (protein)} + G_{SA\ (ligand)})$$

Molecular Dynamics Simulation. Molecular dynamics (MD) simulation study for apo and holo of all complexes were carried out using Desmond.[65] System Builder panel with inbuilt OPLS3 force field was used to build molecular systems. Further solvation was done with TIP3P water molecules using orthorhombic box with distance of 10Å from all sides of protein complex. Orthorhombic box volume was minimized by reorientation of the complex/model system. Appropriate no. of counter Na^+/Cl^- ions were added to electrically neutralize the system. The Steepest descent algorithm with 2000 iterations and convergence threshold of 1 kcal/mol/Å was used to minimize all prepared systems, then further equilibration was performed by using default algorithm which includes two stages of minimization and 4 stages of MD. Finally, 100 ns of molecular dynamics simulation was performed using NPT ensemble with temperature and pressure coupling of 300 K and 1 atm respectively. Coordinates and energy were recorded every 10 ps to yield 10000 frames.[66]

ASSOCIATED CONTENT

* Supplementary information file.

The Supporting Information is available free of charge on the ACS Publications website.

AUTHOR INFORMATION

Corresponding Authors

*SKB.: e-mail, skbanerjee@thsti.res.in; phone, +91 01292876475

*BP.: e-mail, bojapoojary@gmail.com; phone, +91 9686940403

*SA.: e-mail, sasthana@thsti.res.in; phone, +91 01292876489, 8447568689

AUTHOR CONTRIBUTIONS

Shailendra Asthana designed this work. Nikil Purushotham and Boja Poojary performed chemical synthesis, Mrityunjay Singh and Shailendra Asthana performed and designed molecular docking and molecular dynamics simulations studies, Bugga Paramesha and Sanjay K Banerjee performed and supervised experimental assays. All authors wrote this paper and have approved the final version of the manuscript.

[$]Nikil Purushotham, Mrityunjay Singh and Bugga Paramesha contribute equally to this work.

ACKNOWLEDGMENTS

Nikil Purushotham is thankful to DST New Delhi for the INSPIRE fellowship. Mrityunjay Singh and Bugga Paramesha are thankful to Council of Scientific & Industrial Research (CSIR), New Delhi for awarding Senior Research Fellowship and Junior Research Fellowship, respectively. Boja Poojary is thankful to UGC SAP for financial assistance. Sanjay K Banerjee and Shailendra Asthana are thankful to THSTI for providing the necessary support and core funding.

CONFLICTS OF INTERESTS

The authors declare that they do not have any conflicts of interest.

COMPETING FINANCIAL INTERESTS

The author(s) declare no competing financial interest.

Abbreviations:

Sirt1-3: Sirt1, Sirt2 and Sirt3

Sirt1: NAD-dependent protein deacetylase sirtuin-1, Silent information regulator2 homolog 1

Sirt2: NAD-dependent protein deacetylase sirtuin-2, Silent information regulator2 homolog 2

Sirt3: NAD-dependent protein deacetylase sirtuin-3, Silent information regulator2 homolog 3

MD simulation: Molecular Dynamics Simulation

HepG2 cells: Human hepatoma G2, Human liver cancer cell

MCF cells: Michigan Cancer Foundation-7, breast cancer cells

IC_{50}: half maximal inhibitory concentration

HBs: Hydrogen bonds

ESP: Electrostatic surface potential

µM: micro molar

ns: Nano-seconds

h: Hour

MM-GBSA: Molecular Mechanic-Generalized Born Surface Area

RMSD: Root mean Square deviation

RMSF: Root mean square fluctuation

Ex527*: Ex527 analogue with 7-memberd ring

REFERENCES

1. Hsu, W. W.; Wu, B.; Liu, W. R. Sirtuins 1 and 2 Are Universal Histone Deacetylases. *ACS Chemical Biology* **2016,** 11, 792-799.
2. Michan, S.; Sinclair, D. Sirtuins in mammals: insights into their biological function. *Biochemical Journal* **2007,** 404, 1-13.
3. Liu, T.; Liu, P. Y.; Marshall, G. M. The critical role of the class III histone deacetylase SIRT1 in cancer. *Cancer research* **2009,** 69, 1702-1705.
4. Jeong, S. M.; Haigis, M. C. Sirtuins in cancer: a balancing act between genome stability and metabolism. *Molecules and cells* **2015,** 38, 750.
5. Frye, R. A. Phylogenetic classification of prokaryotic and eukaryotic Sir2-like proteins. *Biochemical and biophysical research communications* **2000,** 273, 793-798.
6. Yuan, H.; Marmorstein, R. Structural basis for sirtuin activity and inhibition. *Journal of Biological Chemistry* **2012**, jbc. R112. 372300.
7. Haigis, M. C.; Sinclair, D. A. Mammalian sirtuins: biological insights and disease relevance. *Annual Review of Pathological Mechanical Disease* **2010,** 5, 253-295.
8. Sebastián, C.; Satterstrom, F. K.; Haigis, M. C.; Mostoslavsky, R. From sirtuin biology to human diseases: an update. *Journal of Biological Chemistry* **2012,** 287, 42444-42452.
9. Niederer, F.; Ospelt, C.; Brentano, F.; Hottiger, M. O.; Gay, R. E.; Gay, S.; Detmar, M.; Kyburz, D. SIRT1 overexpression in the rheumatoid arthritis synovium contributes to proinflammatory cytokine production and apoptosis resistance. *Annals of the rheumatic diseases* **2011**, annrheumdis148957.
10. Engler, A.; Tange, C.; Frank-Bertoncelj, M.; Gay, R. E.; Gay, S.; Ospelt, C. Regulation and function of SIRT1 in rheumatoid arthritis synovial fibroblasts. *Journal of Molecular Medicine* **2016,** 94, 173-182.
11. Pinzone, M. R.; Cacopardo, B.; Condorelli, F.; Rosa, M. D.; Nunnari, G. Sirtuin-1 and HIV-1: an overview. *Current drug targets* **2013,** 14, 648-652.
12. Morselli, E.; Maiuri, M.; Markaki, M.; Megalou, E.; Pasparaki, A.; Palikaras, K.; Criollo, A.; Galluzzi, L.; Malik, S.; Vitale, I. Caloric restriction and resveratrol promote longevity through the Sirtuin-1-dependent induction of autophagy. *Cell death & disease* **2011,** 1, e10.
13. Zhao, X.; Allison, D.; Condon, B.; Zhang, F.; Gheyi, T.; Zhang, A.; Ashok, S.; Russell, M.; MacEwan, I.; Qian, Y. The 2.5 Å crystal structure of the SIRT1 catalytic domain bound to nicotinamide adenine dinucleotide (NAD+) and an indole (EX527 analogue) reveals a novel mechanism of histone deacetylase inhibition. *Journal of medicinal chemistry* **2013,** 56, 963-969.
14. Vaziri, H.; Dessain, S. K.; Eaton, E. N.; Imai, S.-I.; Frye, R. A.; Pandita, T. K.; Guarente, L.; Weinberg, R. A. hSIR2SIRT1 functions as an NAD-dependent p53 deacetylase. *cell* **2001,** 107, 149-159.
15. Motta, M. C.; Divecha, N.; Lemieux, M.; Kamel, C.; Chen, D.; Gu, W.; Bultsma, Y.; McBurney, M.; Guarente, L. Mammalian SIRT1 represses forkhead transcription factors. *Cell* **2004,** 116, 551-563.
16. Yeung, F.; Hoberg, J. E.; Ramsey, C. S.; Keller, M. D.; Jones, D. R.; Frye, R. A.; Mayo, M. W. Modulation of NF‐κB‐dependent transcription and cell survival by the SIRT1 deacetylase. *The EMBO journal* **2004,** 23, 2369-2380.
17. Mayoral, R.; Osborn, O.; McNelis, J.; Johnson, A. M.; Izquierdo, C. L.; Chung, H.; Li, P.; Traves, P. G.; Bandyopadhyay, G.; Pessentheiner, A. R. Adipocyte SIRT1 knockout promotes PPARγ activity, adipogenesis and insulin sensitivity in chronic-HFD and obesity. *Molecular metabolism* **2015,** 4, 378-391.
18. Gurd, B. J. Deacetylation of PGC-1α by SIRT1: importance for skeletal muscle function and exercise-induced mitochondrial biogenesis. *Applied Physiology, Nutrition, and Metabolism* **2011,** 36, 589-597.

19. Jeong, J.; Juhn, K.; Lee, H.; Kim, S.-H.; Min, B.-H.; Lee, K.-M.; Cho, M.-H.; Park, G.-H.; Lee, K.-H. SIRT1 promotes DNA repair activity and deacetylation of Ku70. *Experimental & molecular medicine* **2007,** 39, 8.
20. Nogueiras, R.; Habegger, K. M.; Chaudhary, N.; Finan, B.; Banks, A. S.; Dietrich, M. O.; Horvath, T. L.; Sinclair, D. A.; Pfluger, P. T.; Tschöp, M. H. Sirtuin 1 and sirtuin 3: physiological modulators of metabolism. *Physiological reviews* **2012,** 92, 1479-1514.
21. Chang, H.-C.; Guarente, L. SIRT1 and other sirtuins in metabolism. *Trends in Endocrinology & Metabolism* **2014,** 25, 138-145.
22. Chen, H.-C.; Jeng, Y.-M.; Yuan, R.-H.; Hsu, H.-C.; Chen, Y.-L. SIRT1 promotes tumorigenesis and resistance to chemotherapy in hepatocellular carcinoma and its expression predicts poor prognosis. *Annals of surgical oncology* **2012,** 19, 2011-2019.
23. Wang, Z.; Chen, W. Emerging roles of SIRT1 in cancer drug resistance. *Genes & cancer* **2013,** 4, 82-90.
24. Kojima, K.; Ohhashi, R.; Fujita, Y.; Hamada, N.; Akao, Y.; Nozawa, Y.; Deguchi, T.; Ito, M. A role for SIRT1 in cell growth and chemoresistance in prostate cancer PC3 and DU145 cells. *Biochemical and biophysical research communications* **2008,** 373, 423-428.
25. Xia, X.; Zhou, X. Knockdown of SIRT1 inhibits proliferation and promotes apoptosis of paclitaxel-resistant human cervical cancer cells. *Cellular and molecular biology (Noisy-le-Grand, France)* **2018,** 64, 36-41.
26. Asaka, R.; Miyamoto, T.; Yamada, Y.; Ando, H.; Mvunta, D. H.; Kobara, H.; Shiozawa, T. Sirtuin 1 promotes the growth and cisplatin resistance of endometrial carcinoma cells: a novel therapeutic target. *Laboratory Investigation* **2015,** 95, 1363-1373.
27. Choi, H.-K.; Cho, K. B.; Phuong, N. T. T.; Han, C. Y.; Han, H.-K.; Hien, T. T.; Choi, H. S.; Kang, K. W. SIRT1-Mediated FoxO1 Deacetylation Is Essential for Multidrug Resistance-Associated Protein 2 Expression in Tamoxifen-Resistant Breast Cancer Cells. *Molecular Pharmaceutics* **2013,** 10, 2517-2527.
28. Ota, H.; Tokunaga, E.; Chang, K.; Hikasa, M.; Iijima, K.; Eto, M.; Kozaki, K.; Akishita, M.; Ouchi, Y.; Kaneki, M. Sirt1 inhibitor, Sirtinol, induces senescence-like growth arrest with attenuated Ras–MAPK signaling in human cancer cells. *Oncogene* **2006,** 25, 176.
29. Sundriyal, S.; Moniot, S. b.; Mahmud, Z.; Yao, S.; Di Fruscia, P.; Reynolds, C. R.; Dexter, D. T.; Sternberg, M. J.; Lam, E. W.-F.; Steegborn, C. Thienopyrimidinone based sirtuin-2 (SIRT2)-selective inhibitors bind in the ligand induced selectivity pocket. *Journal of medicinal chemistry* **2017,** 60, 1928-1945.
30. Cen, Y. Sirtuins inhibitors: the approach to affinity and selectivity. *Biochimica et Biophysica Acta (BBA)-Proteins and Proteomics* **2010,** 1804, 1635-1644.
31. Dai, H.; Case, A. W.; Riera, T. V.; Considine, T.; Lee, J. E.; Hamuro, Y.; Zhao, H.; Jiang, Y.; Sweitzer, S. M.; Pietrak, B. Crystallographic structure of a small molecule SIRT1 activator-enzyme complex. *Nature communications* **2015,** 6, 1-10.
32. Park, J. B. Finding potent sirt inhibitor in coffee: Isolation, confirmation and synthesis of javamide-II (N-caffeoyltryptophan) as sirt1/2 inhibitor. *PloS one* **2016,** 11.
33. Yoon, Y.; Osman, H.; Choon, T. Potent sirtuin inhibition with 1, 2, 5-trisubstituted benzimidazoles. *MedChemComm* **2016,** 7, 2094-2099.
34. Rumpf, T.; Schiedel, M.; Karaman, B.; Roessler, C.; North, B. J.; Lehotzky, A.; Oláh, J.; Ladwein, K. I.; Schmidtkunz, K.; Gajer, M. Selective Sirt2 inhibition by ligand-induced rearrangement of the active site. *Nature communications* **2015,** 6, 6263.
35. Di Fruscia, P.; Zacharioudakis, E.; Liu, C.; Moniot, S.; Laohasinnarong, S.; Khongkow, M.; Harrison, I. F.; Koltsida, K.; Reynolds, C. R.; Schmidtkunz, K. The Discovery of a Highly Selective 5, 6, 7, 8 -

Tetrahydrobenzo [4, 5] thieno [2, 3 - d] pyrimidin - 4 (3H) - one SIRT2 Inhibitor that is Neuroprotective in an in vitro Parkinson's Disease Model. *ChemMedChem* **2015,** 10, 69-82.
36. Hoffmann, G.; Breitenbücher, F.; Schuler, M.; Ehrenhofer-Murray, A. E. A novel sirtuin 2 (SIRT2) inhibitor with p53-dependent pro-apoptotic activity in non-small cell lung cancer. *Journal of Biological Chemistry* **2014,** 289, 5208-5216.
37. Outeiro, T. F.; Kontopoulos, E.; Altmann, S. M.; Kufareva, I.; Strathearn, K. E.; Amore, A. M.; Volk, C. B.; Maxwell, M. M.; Rochet, J.-C.; McLean, P. J. Sirtuin 2 inhibitors rescue α-synuclein-mediated toxicity in models of Parkinson's disease. *science* **2007,** 317, 516-519.
38. Napper, A. D.; Hixon, J.; McDonagh, T.; Keavey, K.; Pons, J.-F.; Barker, J.; Yau, W. T.; Amouzegh, P.; Flegg, A.; Hamelin, E. Discovery of indoles as potent and selective inhibitors of the deacetylase SIRT1. *Journal of medicinal chemistry* **2005,** 48, 8045-8054.
39. Therrien, E.; Larouche, G.; Nguyen, N.; Rahil, J.; Lemieux, A.-M.; Li, Z.; Fournel, M.; Yan, T. P.; Landry, A.-J.; Lefebvre, S. Discovery of bicyclic pyrazoles as class III histone deacetylase SIRT1 and SIRT2 inhibitors. *Bioorganic & medicinal chemistry letters* **2015,** 25, 2514-2518.
40. Disch, J. S.; Evindar, G.; Chiu, C. H.; Blum, C. A.; Dai, H.; Jin, L.; Schuman, E.; Lind, K. E.; Belyanskaya, S. L.; Deng, J. Discovery of thieno [3, 2-d] pyrimidine-6-carboxamides as potent inhibitors of SIRT1, SIRT2, and SIRT3. *Journal of medicinal chemistry* **2013,** 56, 3666-3679.
41. Ghosh, A.; Sengupta, A.; Seerapu, G. P. K.; Nakhi, A.; Ramarao, E. V. S.; Bung, N.; Bulusu, G.; Pal, M.; Haldar, D. A novel SIRT1 inhibitor, 4bb induces apoptosis in HCT116 human colon carcinoma cells partially by activating p53. *Biochemical and biophysical research communications* **2017,** 488, 562-569.
42. Tae, I. H.; Park, E. Y.; Dey, P.; Son, J. Y.; Lee, S.-Y.; Jung, J. H.; Saloni, S.; Kim, M.-H.; Kim, H. S. Novel SIRT1 inhibitor 15-deoxy-Δ12, 14-prostaglandin J2 and its derivatives exhibit anticancer activity through apoptotic or autophagic cell death pathways in SKOV3 cells. *International journal of oncology* **2018,** 53, 2518-2530.
43. Wang, M.; Rakesh, K.; Leng, J.; Fang, W.-Y.; Ravindar, L.; Gowda, D. C.; Qin, H.-L. Amino acids/peptides conjugated heterocycles: A tool for the recent development of novel therapeutic agents. *Bioorganic chemistry* **2018,** 76, 113-129.
44. Peck, B.; Chen, C.-Y.; Ho, K.-K.; Di Fruscia, P.; Myatt, S. S.; Coombes, R. C.; Fuchter, M. J.; Hsiao, C.-D.; Lam, E. W.-F. SIRT inhibitors induce cell death and p53 acetylation through targeting both SIRT1 and SIRT2. *Molecular cancer therapeutics* **2010**, 1535-7163. MCT-09-0971.
45. Solomon, J. M.; Pasupuleti, R.; Xu, L.; McDonagh, T.; Curtis, R.; DiStefano, P. S.; Huber, L. J. Inhibition of SIRT1 catalytic activity increases p53 acetylation but does not alter cell survival following DNA damage. *Molecular and cellular biology* **2006,** 26, 28-38.
46. Mahajan, S. S.; Scian, M.; Sripathy, S.; Posakony, J.; Lao, U.; Loe, T. K.; Leko, V.; Thalhofer, A.; Schuler, A. D.; Bedalov, A. Development of pyrazolone and isoxazol-5-one cambinol analogues as sirtuin inhibitors. *Journal of medicinal chemistry* **2014,** 57, 3283-3294.
47. Reed, S. M.; Quelle, D. E. p53 acetylation: regulation and consequences. *Cancers* **2015,** 7, 30-69.
48. Yi, J.; Luo, J. SIRT1 and p53, effect on cancer, senescence and beyond. *Biochimica et Biophysica Acta (BBA)-Proteins and Proteomics* **2010,** 1804, 1684-1689.
49. Mellini, P.; Itoh, Y.; Elboray, E. E.; Tsumoto, H.; Li, Y.; Suzuki, M.; Takahashi, Y.; Tojo, T.; Kurohara, T.; Miyake, Y. Identification of Diketopiperazine-Containing 2-Anilinobenzamides as Potent Sirtuin 2 (SIRT2)-Selective Inhibitors Targeting the "Selectivity Pocket", Substrate-Binding Site, and NAD+-Binding Site. *Journal of medicinal chemistry* **2019,** 62, 5844-5862.
50. Chen, L. Medicinal chemistry of sirtuin inhibitors. *Current medicinal chemistry* **2011,** 18, 1936-1946.
51. Du, J.; Zhou, Y.; Su, X.; Yu, J. J.; Khan, S.; Jiang, H.; Kim, J.; Woo, J.; Kim, J. H.; Choi, B. H. Sirt5 is a NAD-dependent protein lysine demalonylase and desuccinylase. *Science* **2011,** 334, 806-809.

52. Jiang, H.; Khan, S.; Wang, Y.; Charron, G.; He, B.; Sebastian, C.; Du, J.; Kim, R.; Ge, E.; Mostoslavsky, R. SIRT6 regulates TNF-α secretion through hydrolysis of long-chain fatty acyl lysine. *Nature* **2013,** 496, 110-113.
53. Roessler, C.; Nowak, T.; Pannek, M.; Gertz, M.; Nguyen, G. T.; Scharfe, M.; Born, I.; Sippl, W.; Steegborn, C.; Schutkowski, M. Chemical probing of the human sirtuin 5 active site reveals its substrate acyl specificity and peptide‐based inhibitors. *Angewandte Chemie International Edition* **2014,** 53, 10728-10732.
54. Schrödinger, L. Schrödinger Release 2017-2: Maestro. *Schrödinger LLC, New York* **2017**.
55. Humphrey, W.; Dalke, A.; Schulten, K. VMD: visual molecular dynamics. *Journal of molecular graphics* **1996,** 14, 33-38.
56. Mills, N. ChemDraw Ultra 10.0 CambridgeSoft, 100 CambridgePark Drive, Cambridge, MA 02140. www. cambridgesoft. com. Commercial Price: 1910fordownload, 2150 for CD-ROM; Academic Price: 710fordownload, 800 for CD-ROM. In ACS Publications: 2006.
57. Release, S. 1: Desmond molecular dynamics system, version 3.7. *DE Shaw Research, New York, NY, Maestro-Desmond Interoperability Tools, version* **2014,** 3.
58. Harder, E.; Damm, W.; Maple, J.; Wu, C.; Reboul, M.; Xiang, J. Y.; Wang, L.; Lupyan, D.; Dahlgren, M. K.; Knight, J. L. OPLS3: a force field providing broad coverage of drug-like small molecules and proteins. *Journal of chemical theory and computation* **2016,** 12, 281-296.
59. Repasky, M. P.; Shelley, M.; Friesner, R. A. Flexible ligand docking with Glide. *Current protocols in bioinformatics* **2007,** 18, 8.12. 1-8.12. 36.
60. Asthana, S.; Zucca, P.; Vargiu, A. V.; Sanjust, E.; Ruggerone, P.; Rescigno, A. Structure-Activity Relationship Study of Hydroxycoumarins and Mushroom Tyrosinase. *Journal of agricultural and food chemistry* **2015,** 63, 7236-44.
61. Mattapally, S.; Singh, M.; Murthy, K. S.; Asthana, S.; Banerjee, S. K. Computational modeling suggests impaired interactions between NKX2.5 and GATA4 in individuals carrying a novel pathogenic D16N NKX2.5 mutation. *Oncotarget* **2018,** 9, 13713-13732.
62. Mittal, L.; Kumari, A.; Suri, C.; Bhattacharya, S.; Asthana, S. Insights into structural dynamics of allosteric binding sites in HCV RNA-dependent RNA polymerase. *Journal of biomolecular structure & dynamics* **2020,** 38, 1612-1625.
63. Li, J.; Abel, R.; Zhu, K.; Cao, Y.; Zhao, S.; Friesner, R. A. The VSGB 2.0 model: a next generation energy model for high resolution protein structure modeling. *Proteins: Structure, Function, and Bioinformatics* **2011,** 79, 2794-2812.
64. Mittal, L.; Srivastava, M.; Asthana, S. Conformational Characterization of Linker Revealed the Mechanism of Cavity Formation by 227G in BVDV RDRP. *The Journal of Physical Chemistry B* **2019,** 123, 6150-6160.
65. Srivastava, M.; Suri, C.; Singh, M.; Mathur, R.; Asthana, S. Molecular dynamics simulation reveals the possible druggable hot-spots of USP7. *Oncotarget* **2018,** 9, 34289.
66. Subramanian, L.; Maghajothi, S.; Singh, M.; Kesh, K.; Kalyani, A.; Sharma, S.; Khullar, M.; Victor, S. M.; Swarnakar, S.; Asthana, S.; Mullasari, A. S.; Mahapatra, N. R. A Common Tag Nucleotide Variant in MMP7 Promoter Increases Risk for Hypertension via Enhanced Interactions With CREB (Cyclic AMP Response Element-Binding Protein) Transcription Factor. *Hypertension (Dallas, Tex. : 1979)* **2019,** 74, 1448-1459.

Abstract graphics

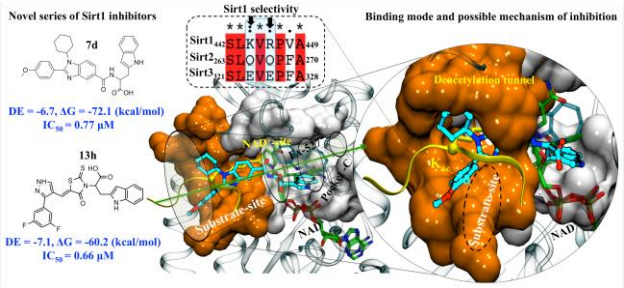

Scheme 1: Synthetic strategy for the benzimidazole monopeptides[a].(**7a-l**)

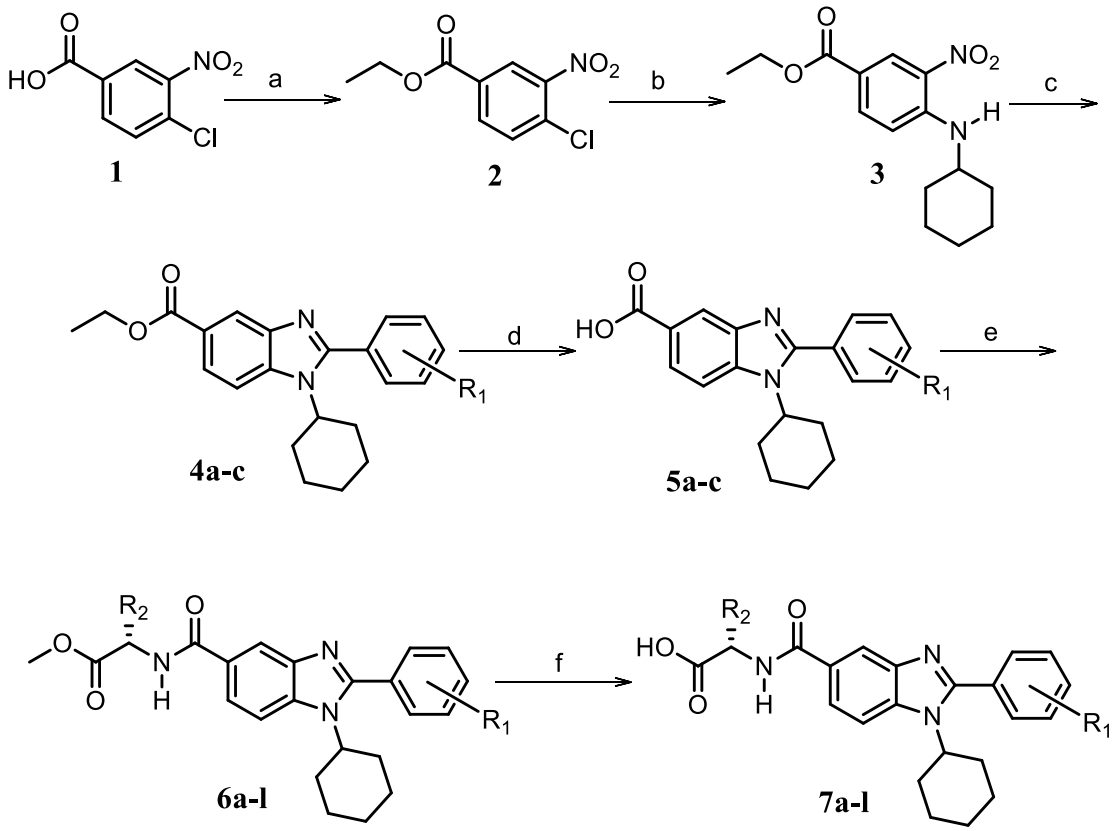

[a]**Reagents and conditions:** (a) EtOH, conc. H_2SO_4 (catalytic), reflux; (b) Cyclohexylamine (2.5 equiv.), TEA (3.0 equiv.), THF, r.t.; (c) Substituted benzaldehyde (1 equiv.), $Na_2S_2O_4$ (3 equiv.), DMSO, 90 °C; (d) NaOH (1.1 eqiv.), water, reflux; (e) Amino acid methyl ester hydrochloride (1 equiv.), NMM (2.5 equiv.), TBTU (1.25 equiv.), DMF, r.t.; (f) $LiOH.H_2O$ (1 equiv.), water:THF (2:1), 0 °C.

R_1*= 4-F, 4-OCH_3, 2-Cl-6-F; R_2*= CH_3, $CH(CH_3)_2$, CH_2-$CH(CH_3)_2$, 3-indolylmethyl.

*Further for substitution pattern see **Table 1**

Scheme 2: Synthetic strategy for the preparation of pyrazole conjugated rhodanine carboxylic acids[a]. **(13a-l)**

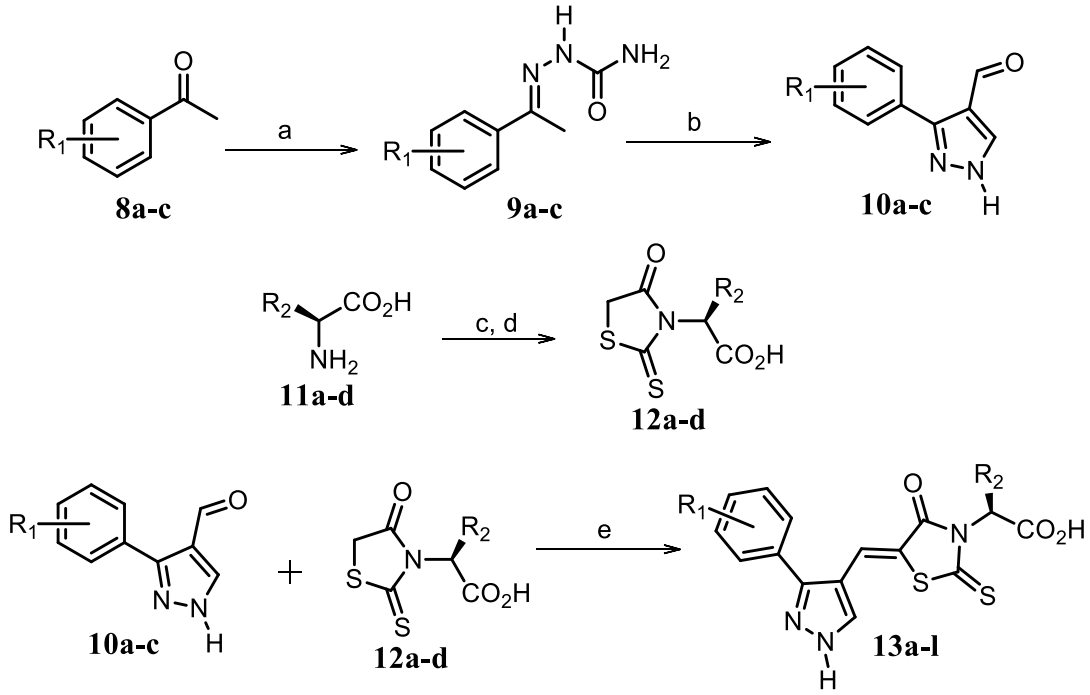

[a]**Reagents and conditions:** (a) Semicarbazide hydrochloride (1.1 equiv.), NaOAc (1.3 equiv.), EtOH, reflux; (b) $POCl_3$ (10 equiv.), reflux; (c) CS_2 (1.2 equiv.), KOH (1 equiv.), water, rt; (d) Potassium chloroacetate (1 equiv.), 2N HCl till pH 2, 90 °C; (e) β-alanine (2 equiv.), AcOH, reflux. R_1^* = 4-OCH_3, 4-NO_2, 3,5-F_2; R_2^* = H, CH_3, CH_2-C_6H_5, 3-indolylmethyl.

*Further for substitution pattern see **Table 2**.

Figures:

Figure 1: Representative reported structure of sirtuin inhibitors with their IC_{50} values. The carboxamide functionality and benzimidazole/pyrazole/indole scaffolds are highlighted in bold blue color, while region for selectivity are marked with dotted circle.

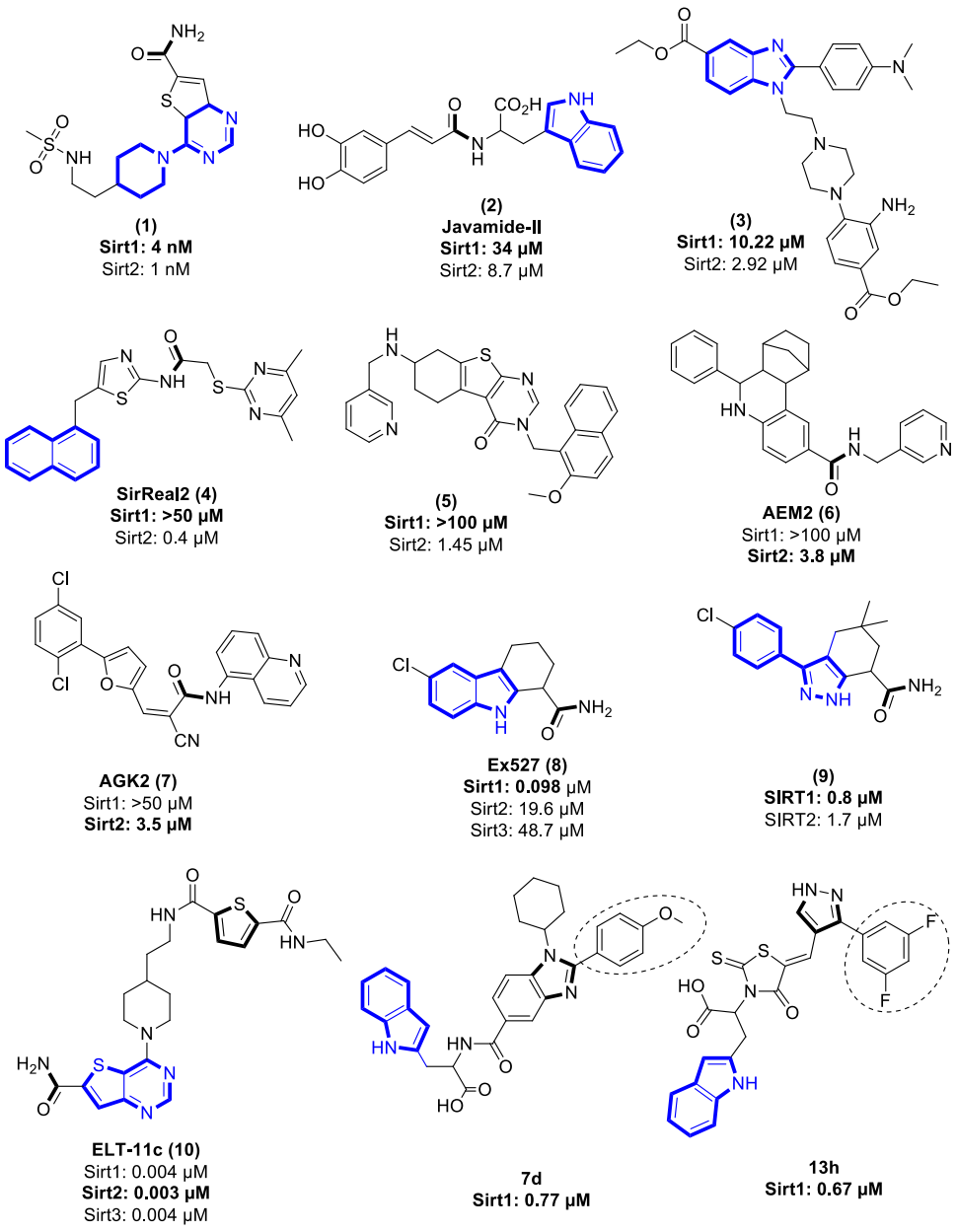

Figure 2. Architecture of Sirt1 catalytic site: A) Structure of Human Sirt1 with Inhibitor Ex527-analogue (Ex527*) and co-factor NAD, "PDB id: 4I5I". In right-inset enlarged surface view of catalytic grove (cut-off distance 6.0 Å), with Ex527*, NAD+ and docked Ex527. NAD+ is shown in licorice representation rendered in atom wise i.e carbon atom in cyan color, while Ex527* and Ex527 are shown in ball and sticks representation in which carbon atoms are in cyan and green color, respectively. B) Heat map of MM-GBSA and docking score of all designed compounds docked on Sirt1, Sirt2 and Sirt3. The cut-off scores is highlighted with dotted black box. All ligand are represented in the form of small square, colour of square represent respective colour of MM-GBSA heat-map. Ligand 7d, 13d, 13h and 13l are marked with arrows in left most panel.

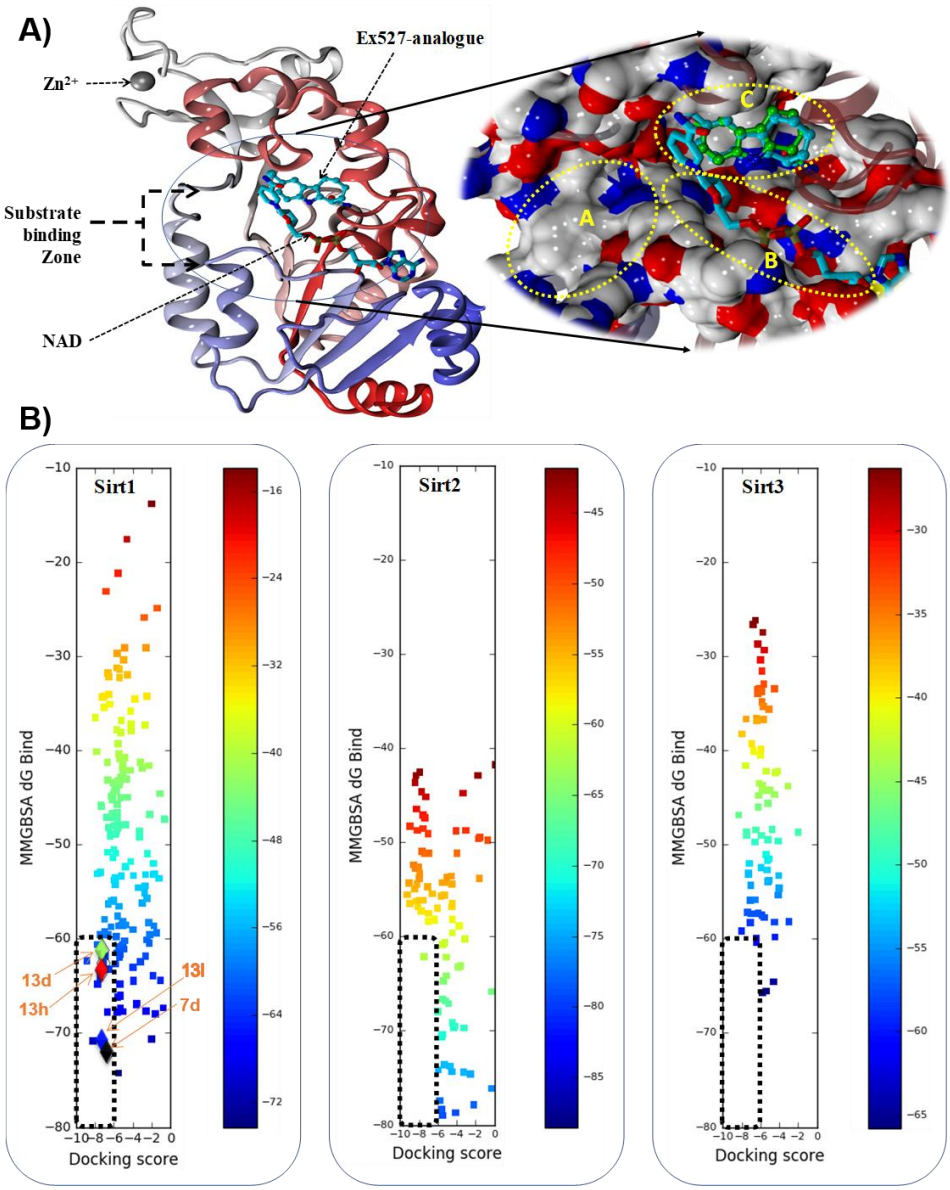

Figure 3. *In-vitro* evaluation of computationally promising compounds: (A&B) The % viability of cancer cells in the presence of test compounds at different concentrations. Results were represented as mean ± SEM, n=3. **(A)** Assay in HepG2 cell, **(B)** Assay in MCF7 cells. (**C)** Immune blotting shows the effect of control and test compounds on protein expression of Ac-p53 in HepG2 cells.

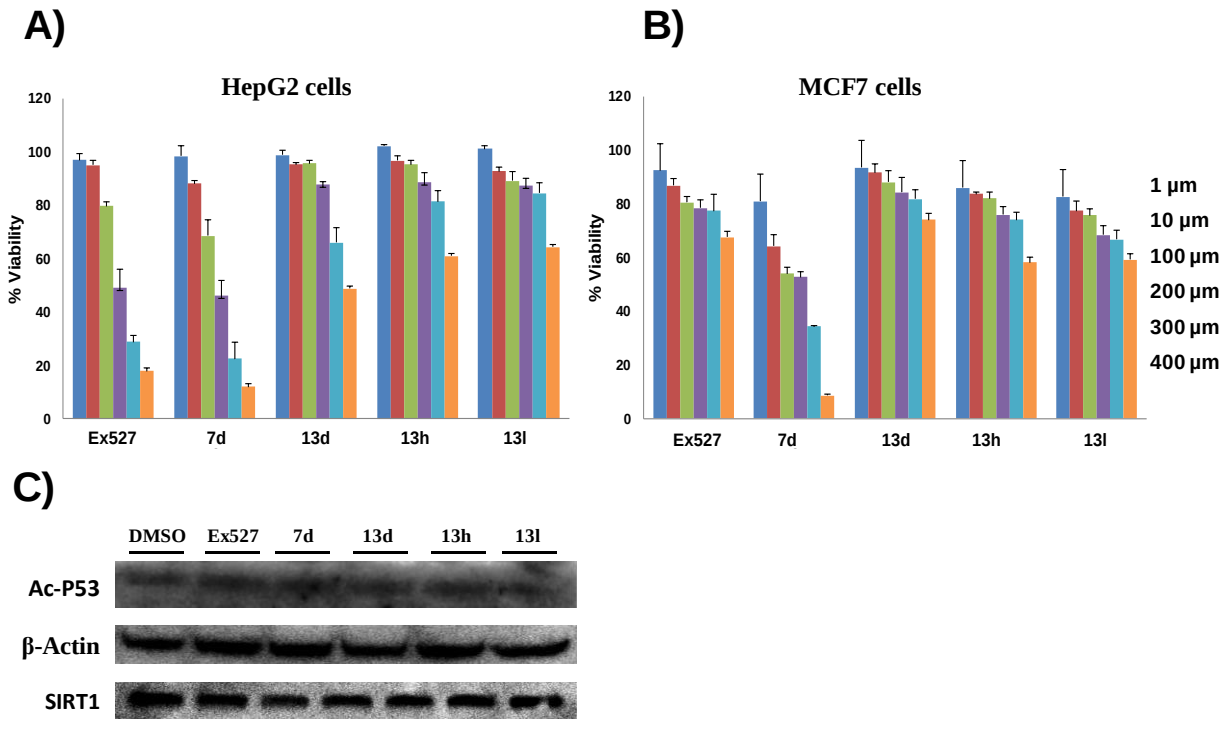

Figure 4. Molecular dynamics simulations reflects the significant changes in ligand behavioural pattern: (A & B) MD trajectory analysis of Apo Sirt1 and Protein-Ligand complexes of 7d, 13d, 13h and 13l. **(A)** The Root mean square deviation (RMSD), of protein (all backbone atoms) and ligand in coordinates as a function of the simulation time. **(B)** The Root mean square fluctuation (RMSF) and ΔRMSF of C-alpha atoms of MD systems, Sirt1-apo, Sirt1-Ex527* and Sirt1-7d. **(C)** Per-residue energy decomposition of Ex527*, 7d and 13d. The residue which reflected the major contribution in binding free energies ($\Delta G_{pbsa} \leq$ -0.5 kcal/mol) is shown in the graphs. The region highlighted with pink color background belongs to substrate binding site. **(D)** The interaction map of 7d, 13d, 13h, 13l. The ligand 7d, 13d, 13h and 13l are shown in representation "stick" in color-type "element" with "C" in fluorescent cyan. The key residue within 3.5 Å cutoff from ligands are highlighted in color-type "element" with "C" in pink color. The C-alpha atom and side chain are shown in "sphere" and "stick" representation, respectively. Backbone atoms showed for only those residues, which involved in HBs interaction. Backbone atoms are shown in stick representation. Water (oxygen atom) within 2.5 Å from ligand is shown in sphere representation in red color. HBs are shown with dotted line and green color.

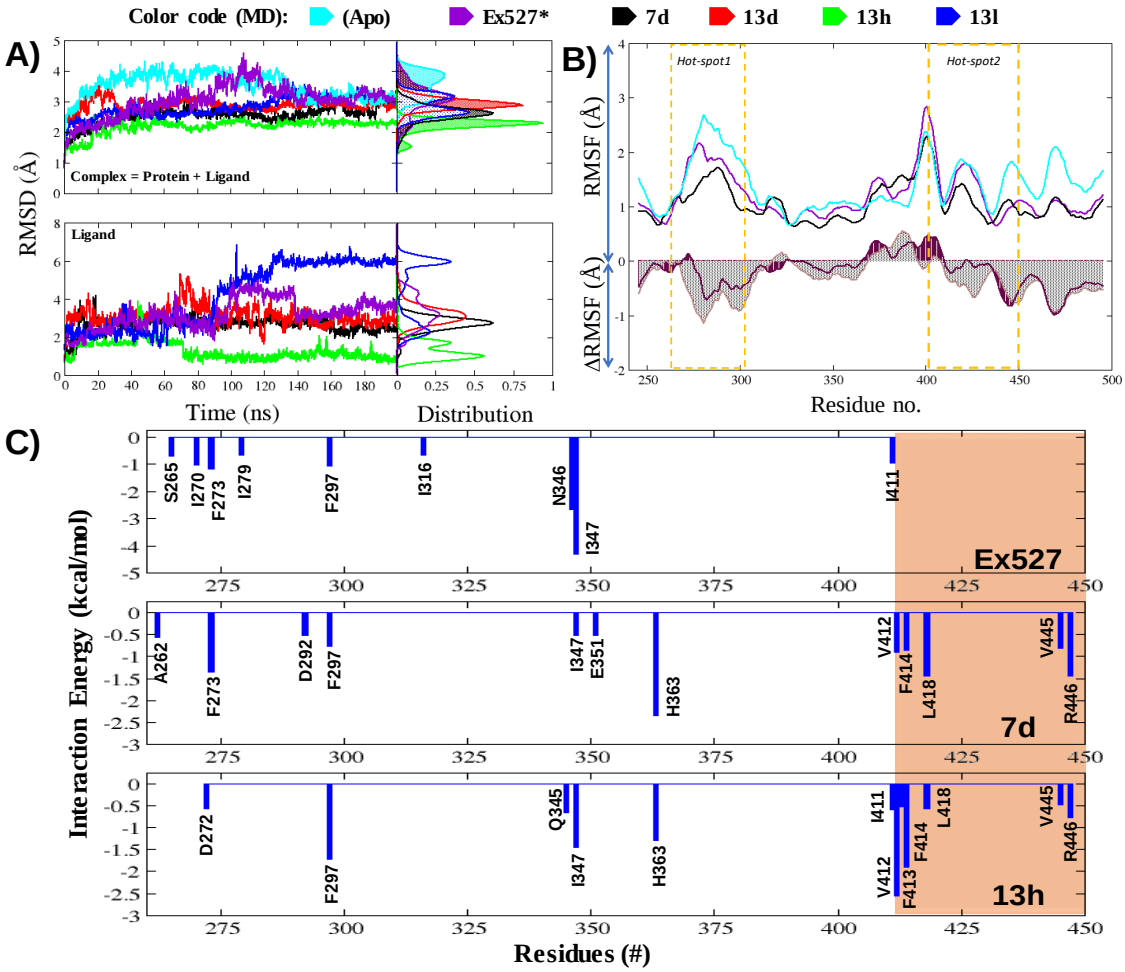
Color code (MD): (Apo) Ex527* 7d 13d 13h 13l
A)
RMSD (Å)
Complex = Protein + Ligand
Ligand
Time (ns)
Distribution
B)
Hot-spot1
Hot-spot2
RMSF (Å)
ΔRMSF (Å)
Residue no.
C)
Interaction Energy (kcal/mol)
Ex527
7d
13h
Residues (#)
D)
7d
13d
13h
13l

Figure 5. Establishment of SAR of Scheme1 compounds and their Molecular dynamics simulations to reflects the structural differences: **(A)** Binding of scheme1 (Table 2) inhibitor (stick representation), with –OMe substitution in R1 position, in catalytic pocket of Sirt1. The compound 7d shown in representation sticks and color-type element with C in green, while rest other compounds are shown in representation sticks, color-type 7a in yellow color, 7b in violet color and 7c in orange color. **(B)** Overlay binding of compounds 7l-7d, and 7h-7d at catalytic pocket to speculate the difference in their binding pose. Sirt1 catalytic pocket is shown in surface view. 7d is shown in representation "stick" in color-type "element" with "C" in fluorescent green, while compound 7l and 7h are shown in representation "ball and stick" in colour-type "element with "C" in green. The zone of interest are highlighted with yellow circle. **(C)** MD trajectory analysis of scheme1 molecules (7l, 7h and 7d). The Root mean square deviation (RMSD) of protein (all backbone atoms) and ligand (no hydrogen atom) in coordinates as a function of the simulation time.

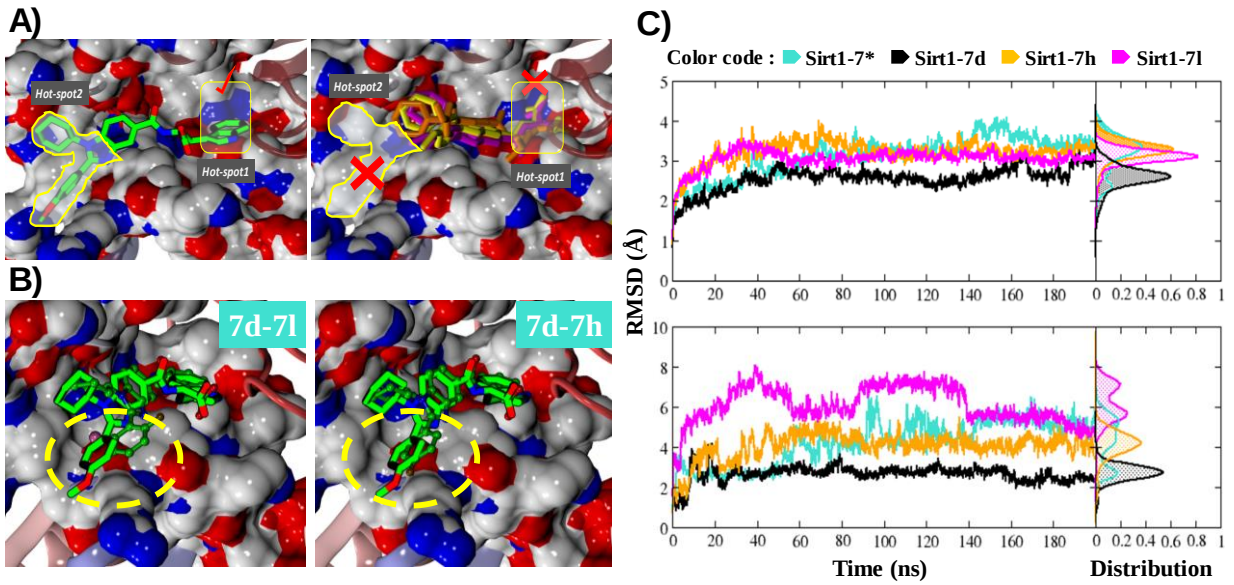

Figure 6. Selectivity at substrate binding site explored at sequence and structural level: (A) The sequence alignment of Sirt1, Sirt2 and Sirt3 PDB id. 4I5I, 4RMG and 4JSR, respectively. The region highlighted in cyan and deep cyan color represent substrate binding zone. **(B)** The enlarged view of the sequence alignment of lower panel of substrate binding zone of Sirt1-3 (green color box). The arrow sign marked the residues K444 and R446 playing key role in Sirt1 selectivity of 7d via polar electrostatic interaction. (**C** and **D**) Electrostatic Surface view of ligand 7d (C) and Sirt1 binding cavity (D). **(E-G)** The electrostatic surface potential (ESP) complementarity analysis of 7d with, Sirt1 **(E)**, Sirt2 **(F)** and Sirt3 **(G)**. Protein is shown in solid surface while 7d is shown in mesh surface. The blue and red color surface represent positive and negative potential, respectively. The region highlighted with green dotted circle highlights the selectivity zone at substrate site.

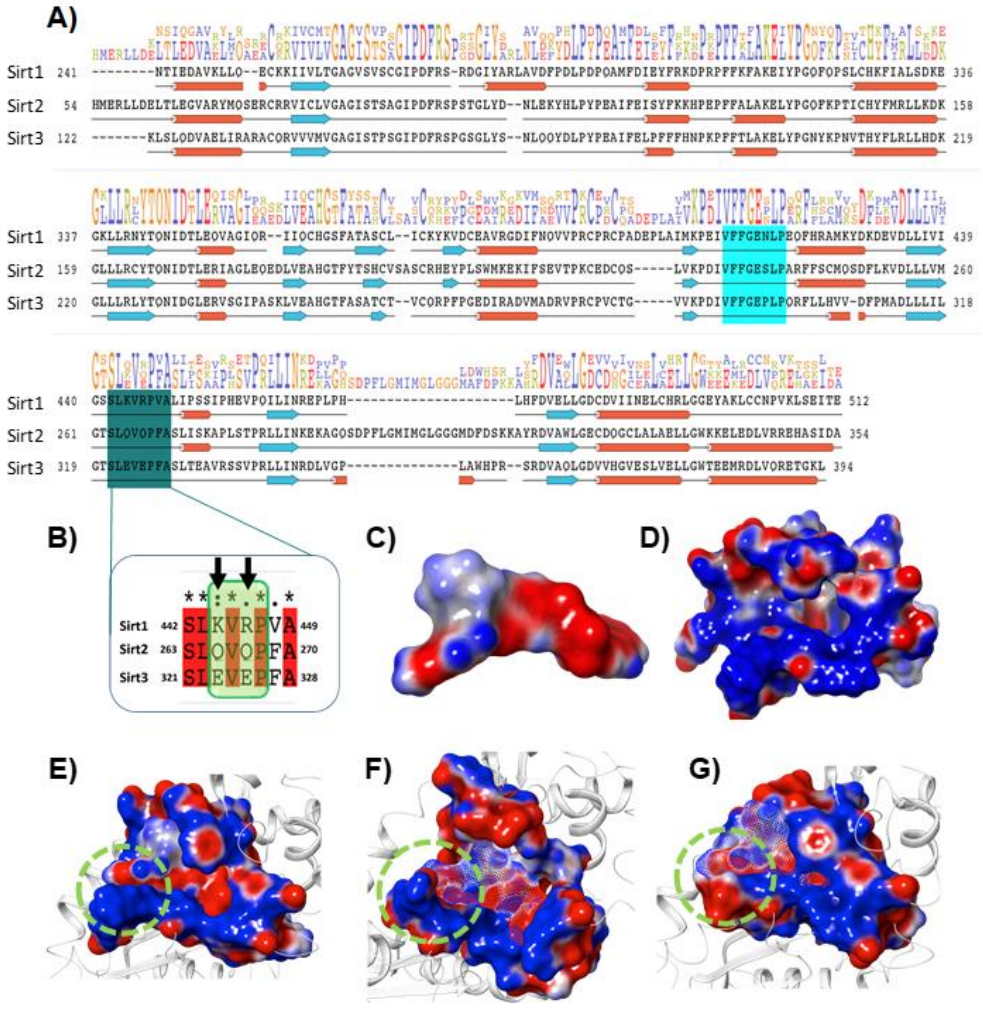

Tables:

Table 1. Structure of Scheme1 compounds with their elemental property, docking score, MM-GBSA binding energy and enzyme-based inhibition activity. The biological evaluation of enzyme-based inhibitory activity of test compounds at 10 µm concentration was obtained against recombinant human Sirt1, Sirt2 and Sirt3.

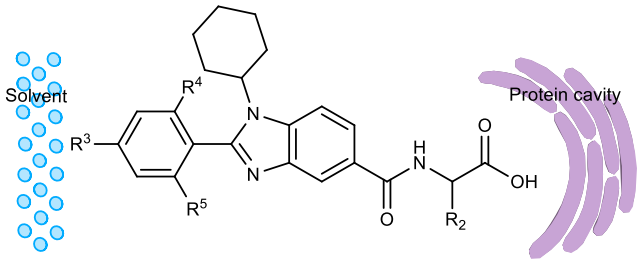

Comp.	R_2	R^3	R^4/R^5	Mol. mass	cLogP	Dock Score (Sirt1)	ΔG_{bind} (S	% inhibition at 10 µM		
								Sirt1	Sirt2	Sirt3
7a	$-CH_3$	–OMe	–H	421	5.05	-6.26	-58.96	88.03	-59.54	-112.65
7b		–OMe	–H	450	5.98	-7.06	-59.49	88.18	-84.09	-88.31
7c		–OMe	–H	464	6.51	-6.68	-58.85	86.34	-37.06	-127.63
7d		–OMe	–H	537	6.46	-6.70	-72.08	89.99	-13.81	-104.72
7e	$-CH_3$	–F	–H	409	5.18	-6.51	-54.45	<50	-	-
7f		–F	–H	437	6.11	-7.40	-54.66	<50	-	-
7g		–F	–H	451	6.64	-6.08	-58.20	88.82	-76.30	-80.68
7h	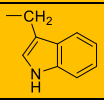	–F	–H	525	6.59	-5.84	-61.60	86.83	-25.70	-99.31
7i	$-CH_3$	–H	–Cl/F	472	6.58	-7.08	-49.04	<50	-	-
7j		–H	–Cl/F	486	7.11	-5.33	-33.49	<50	-	-
7k		–H	–Cl/F	559	7.05	-6.61	-56.97	<50	-	-
7l	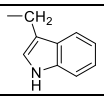	–H	–Cl/F	559	7.05	-6.61	-56.97	<50	-	-

*highlights are showing ligands selected for further biological and MD studies on basis of cut-off score (docking score ≤ -6.0 and ΔG_{bind} ≤ -60.0 kcal/mol).

Table 2. Structure of Scheme2 compounds with their elemental property, docking score, MM-GBSA binding energy (ΔG_{bind}) and enzyme-based inhibition activity. The biological evaluation of enzyme-based inhibitory activity of test compounds at 10 µm concentration was obtained against recombinant human Sirt1, Sirt2 and Sirt3.

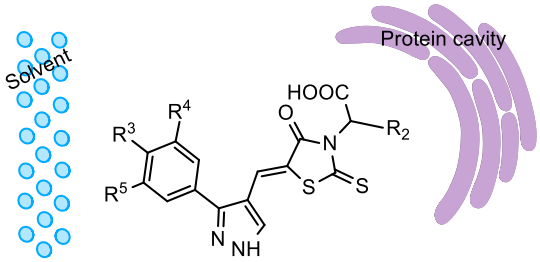

Comp.	R	R_1	R_2/R_3	Mol. Mass	cLogP	Dock Score (Sirt1)	ΔG_{bind} (Sirt1)	% inhibition at 10 µM		
								Sirt1	Sirt2	Sirt3
13a	–H	–OMe	–H	375.42	1.65	-6.537	-47.191	-	-	-
13b	$-CH_3$	–OMe	–H	389.44	1.96	-6.176	-46.735	-	-	-
13c	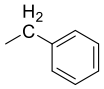	–OMe	–H	465.08	3.38	-7.436	-40.642	-	-	-
13d	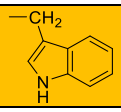	–OMe	–H	504.58	3.37	-7.258	-63.4	90.64	-41.54	-48.19
13e	–H	–H	–F	381.37	1.97	-6.36	-48.847	-	-	-
13f	$-CH_3$	–H	–F	395.40	2.28	-6.511	-48.219	-	-	-
13g	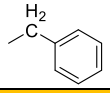	–H	–F	471.50	3.7	-7.42	-52.957	-	-	-
13h	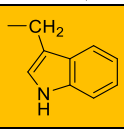	–H	–F	510.53	3.69	-7.206	-60.234	89.15	-17.73	-46.05
13i	–H	$-NO_2$	–H	390.39	1.46	-6.971	-59.301	-	-	-
13j	$-CH_3$	$-NO_2$	–H	404.42	1.77	-7.699	-53.106	-	-	-
13k		$-NO_2$	–H	480.51	3.19	-6.267	-56.012	-	-	-
13l	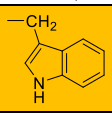	$-NO_2$	–H	519.55	3.18	-7.088	-70.882	89.64	-24.59	-34.51

*highlights are showing ligands selected for further biological and MD studies on basis of cut-off score (docking score ≤ -6.0 and ΔG_{bind} ≤ -60.0 kcal/mol).

Table 3: Determination of cell-based inhibitory activity and IC_{50} of test compounds and control. The cell-based inhibitory activity was estimated at 10 µM concentration in HepG2 cells against Sirt1 and Sirt2/3. IC_{50} values are calculated in human recombinant Sirt1. Results were represented as mean ± SEM, n=3.

Comp.	% Inhibition of Sirt1	% Inhibition of Sirt2 and Sirt3	IC_{50} (µM) Sirt1
7a	<1	-	-
7b	<1	-	-
7c	3.235±0.2799	5.21±0.785	-
7d	38.333±0.3719	19.89±0.895	0.77+0.04
7g	<1	-	-
7h	<1	-	-
13d	36.338±0.9965	6.04±0.915	0.71+0.03
13h	48.540±0.9175	9.53±0.654	0.66+0.02
13l	30.061±0.2338	9.47±0.9236	0.73+0.06
Ex527[#]	33.330±0.647	15.21±0.9985	0.60+0.02

[#]biological assay control or standard compound.
*Highlights are showing compounds with highest Sirt1 inhibition.